

was heated under reflux for 3 h and then was cooled to 23 °C. The solvent was removed and the aqueous phase was extracted with CHCl₃. The organic extracts were dried (Na₂SO₄), and the solvent was removed. Flash-chromatography of the residue (1:4 EtOAc/hexanes) afforded 16 mg (38%) of *O*-benzyl-3,9-dioxo-6-thiacyclodecan-1-ol as a colorless oil. ¹H NMR (CDCl₃) δ 7.36–7.27 (m, 5H), 4.59 (s, 2H), 3.90–3.85 (m, 2H), 3.82–3.48 (m, 7H), 2.91–2.74 (m, 4H). ¹³C NMR (CDCl₃) δ 133.5, 128.3, 127.7, 126.0, 75.9, 71.9, 71.6, 68.0, 33.4. MS (ESI) *m/z* 291 [M + Na]⁺, 286 [M + H + NH₄]⁺, 269 [M + H]⁺. To a solution of the above compound (11 mg, 0.040 mmol) in CH₂Cl₂ (2 mL), cooled to 0 °C, *m*-chloroperbenzoic acid (77%, 22 mg, 0.09 mmol) was added in small portions. After 18 h, a 1% solution of sodium bisulfite was added, the layers were separated, and the organic phase was washed with a saturated solution of NaHCO₃. The organic extracts were dried (Na₂SO₄) and evaporated. The residue was purified by flash-chromatography (1:4 EtOAc/CHCl₃) to afford 11 mg (93%) of **22** as a brown oil. ¹H NMR (CDCl₃) δ 7.37–7.29 (m, 5H), 4.57 (s, 2H), 4.01–3.96 (m, 4H), 3.77–3.72 (m, 1H), 3.66–3.60 (m, 4H), 3.40–3.38 (m, 2H), 3.34–3.23 (m, 2H). ¹³C NMR (CDCl₃) δ 133.4, 128.4, 127.9, 127.7, 74.7, 71.8, 66.4, 64.6, 52.4.

3,9-Dioxo-6-thiacyclodecan-1-ol-6,6-dioxide (8). A mixture of **22** (25 mg, 0.083 mmol) and a catalytic amount of 10% Pd/C in EtOAc (3 mL) was stirred at 23 °C under a hydrogen atmosphere. After 48 h, the catalyst was filtered off and the filtrate was evaporated to afford 16 mg (92%) of **8** as a colorless oil. ¹H NMR (CDCl₃) δ 4.08–3.95 (m, 4H), 3.67 (dd, *J* = 4.2, 9.9 Hz, 2H), 3.61–3.59 (m, 1H), 3.51 (dd, *J* = 5.7, 9.9 Hz, 2H), 3.38–3.23 (m, 4H). ¹³C NMR (CDCl₃) δ 69.0, 68.3, 64.5, 52.6.

O,6-Dibenzyl-3,9-dioxo-6-azocyclodecan-1-ol (23). A mixture of **21**²⁴ (150 mg, 0.37 mmol), benzylamine (41 μL, 0.37 mmol), lithium perchlorate (340 mg, 3.7 mmol), and sodium carbonate (200 mg, 1.9 mmol) in acetonitrile (7.5 mL) was heated under reflux for 48 h. After cooling to 23 °C, the solvent was removed, the residue was suspended in CHCl₃, and the organic phase was washed with water and dried (Na₂SO₄). Flash-chromatography of the residue (2:1 EtOAc/CHCl₃) afforded 31 mg (24%) of **23** as a colorless oil. ¹H NMR (CDCl₃) δ 7.36–7.20 (m, 10H), 4.59 (s, 2H), 3.87–3.78 (m, 4H), 3.69 (s, 2H), 3.67–3.49 (m, 5H), 2.91–2.72 (m, 4H). MS (ESI) *m/z* 342 [M + 1]⁺.

***N*-(tert-Butoxycarbonyl)-3,9-dioxo-6-azocyclodecan-1-ol (24)**. A mixture of **23** (40 mg, 0.12 mmol), Boc₂O (26 mg, 0.12 mmol), and a catalytic amount of 10% Pd/C in EtOAc (3 mL) was stirred at 23 °C under a hydrogen atmosphere. After 18 h, the catalyst was filtered off and the filtrate was evaporated to afford 26 mg (95%) of **24** as a colorless oil. ¹H NMR (CDCl₃) δ 3.83–3.70 (m, 7H), 3.65–3.59 (m, 2H), 3.49–3.29 (m, 4H), 1.75 (bs, 1H), 1.46 (s, 9H). ¹³C NMR (CDCl₃) δ 155.7, 79.8, 71.4, 71.0, 70.3, 69.9, 50.5, 50.2, 28.5.

(*S*)-1-(4-Nitrophenoxy)carbonyloxy-3,5-dioxacyclooctane (25a). To a solution of **8a** (15 mg, 0.11 mmol) and *N*-methylmorpholine (38 μL, 0.34 mmol) in dry THF (3 mL), *p*-nitrophenylchloroformate (70 mg, 0.28 mmol) was added and the resulting mixture was stirred at 23 °C for 1 h. To the reaction mixture was added water, the solvent was removed under reduced pressure, and the aqueous phase was extracted with CHCl₃. The organic extracts were dried (Na₂SO₄), and the solvent was removed. The residue was purified by flash-chromatography (1:4 EtOAc/CHCl₃) to afford 28 mg (81%) of **25a** as a pale-yellow solid. ¹H NMR (CDCl₃) δ 8.27 (d, *J* = 9.3 Hz, 2H), 7.38 (d, *J* = 9.3 Hz, 2H), 5.09–5.01 (m, 1H), 4.72–4.66 (m, 2H), 3.94–3.82 (m, 3H), 3.64–3.56 (m, 1H), 2.18–2.04 (m, 1H), 2.03–1.93 (m, 2H), 1.90–1.71 (m, 1H).

(*S*)-1-(4-Nitrophenoxy)carbonyloxy-3,5-dioxacycloheptane (25b). The title compound was obtained from (*S*)-**8b** as described for **25a** in 72% yield. Flash-chromatography was performed using a 1:5 mixture of EtOAc and CHCl₃ as the eluant. ¹H NMR (CDCl₃) δ 8.28 (d, *J* = 9.3 Hz, 2H), 7.40 (d, *J* = 9.3 Hz, 2H), 5.00–4.98 (m, 1H), 4.84 (d, *J* = 4.5 Hz, 1H), 4.79 (d, *J* = 4.5 Hz, 1H), 4.11 (dd, *J* = 4.7, 13.1 Hz, 1H), 3.99–3.90 (m, 2H), 3.85–3.78 (m, 1H), 2.19–2.04 (m, 2H).

(*R*)-1-(4-Nitrophenoxy)carbonyloxy-3,5-dioxacyclooctane (25c). The title compound was obtained from (*R*)-**8c** as described for **25a** in 87% yield after flash-chromatography (1:4 EtOAc/CHCl₃). ¹H NMR data are consistent with those reported for the (*S*)-enantiomer **25a**.

(*R*)-1-(4-Nitrophenoxy)carbonyloxy-3,5-dioxacycloheptane (25d). The title compound was obtained from (*R*)-**8d** as described for **25a** in 70% yield after flash-chromatography (1:5 EtOAc/CHCl₃). ¹H data are consistent with those reported for the (*S*)-enantiomer **25b**.

(*R*)-3-(4-Nitrophenoxy)carbonyloxyoxepane (25e). The title compound was obtained from **8e** as described for **25a** in 86% yield. Flash-chromatography was performed using a 1:20 mixture of EtOAc and CHCl₃ as the eluant. ¹H NMR (CDCl₃) δ 8.26 (d, *J* = 9.3 Hz, 2H), 7.38 (d, *J* = 9.3 Hz, 2H), 5.02–4.95 (m, 1H), 3.98–3.83 (m, 3H), 3.71–3.63 (m, 1H), 2.15–1.74 (m, 5H), 1.65–1.53 (m, 1H).

(*S*)-4-(4-Nitrophenoxy)carbonyloxyoxepane (25f). The title compound was obtained from **8f** as described for **25a** in 77% yield. Flash-chromatography was performed using a 1:20 mixture of EtOAc and CHCl₃ as the eluant. ¹H NMR (CDCl₃) δ 8.27 (d, *J* = 8.8 Hz, 2H), 7.36 (d, *J* = 8.8 Hz, 2H), 5.05–5.01 (m, 1H), 3.84–3.62 (m, 4H), 2.18–1.86 (m, 5H), 1.78–1.63 (m, 1H).

1-(4-Nitrophenoxy)carbonyloxy)cycloheptane (25g). The title compound was obtained from commercially available cycloheptanol as described for **25a** in 89% yield. Flash-chromatography was performed using a 1:10 mixture of EtOAc and CHCl₃ as the eluant. ¹H NMR (CDCl₃) δ 8.26 (d, *J* = 8.7 Hz, 2H), 7.37 (d, *J* = 8.7 Hz, 2H), 4.96–4.89 (m, 1H), 2.08–2.02 (m, 2H), 1.86–1.78 (m, 2H), 1.71 (m, 2H), 1.59 (m, 4H), 1.40–1.36 (m, 2H).

5-(4-Nitrophenoxy)carbonyloxy-1,3-dioxane (25h). The title compound was obtained from **8h** as described for **25a** in 72% yield. Flash-chromatography was performed using a 1:4 mixture of EtOAc and CHCl₃ as the eluant. ¹H NMR (CDCl₃) δ 8.30 (d, *J* = 8.7 Hz, 2H), 7.42 (d, *J* = 8.7 Hz, 2H), 5.03 (d, *J* = 6.3 Hz, 1H), 4.87 (d, *J* = 6.3 Hz, 1H), 4.71 (t, *J* = 2.8 Hz, 1H), 4.19–4.06 (m, 4H).

3,6,9-Trioxo-1-cyclodecanol succinimidylcarbonate (25i). To a solution of **8i** (18 mg, 0.11 mmol) in dry acetonitrile (1 mL), *N,N'*-disuccinimidyl carbonate (43 mg, 0.17 mmol) and triethylamine (32 μL, 0.23 mmol) were added and the resulting mixture was stirred at 23 °C. After 8 h, the solvent was removed, the residue was taken up in a saturated solution of NaHCO₃, and the aqueous phase was extracted with EtOAc. The organic extracts were dried (Na₂SO₄), and the solvent was removed in vacuo. Purification of the residue (10:1 EtOAc/MeOH) afforded **17b** (13 mg) in 37% yield. ¹H NMR (CDCl₃) δ 5.12–5.03 (m, 1H), 3.96–3.65 (m, 12H), 2.81 (s, 4H).

12-(4-Nitrophenoxy)carbonyloxy-1,4,7,10-tetraoxacyclotridecane (25j). The title compound was obtained from **8j** as described for **25a** in 70% yield after flash-chromatography (EtOAc). ¹H NMR (CDCl₃) δ 8.27 (d, *J* = 9.3 Hz, 2H), 7.39 (d, *J* = 9.3 Hz, 2H), 5.15–5.08 (m, 1H), 3.92 (dd, *J* = 6.3, 10.2 Hz, 2H), 3.82 (dd, *J* = 4.5, 10.2 Hz, 2H), 3.74–3.60 (m, 12H).

9-(4-Nitrophenoxy)carbonyloxy-1,7-dioxo-4-thiacyclodecane 4,4-dioxide (25k). The title compound was obtained from **8k** as described for **25a** in 73% yield after flash-chromatography (1:4 EtOAc/CHCl₃). ¹H NMR (CDCl₃) δ 8.28 (d, *J* = 9.0 Hz, 2H), 7.37 (d, *J* = 9.0 Hz, 2H), 5.10–5.03 (m, 1H), 4.13–4.06 (m, 4H), 3.83–3.73 (m, 4H), 3.43–3.22 (m, 4H).

11-(4-Nitrophenoxy)carbonyloxy-1,4,6,9-tetraoxacyclododecane (25l). The title compound was obtained from **8l** as described for **25a** in 67% yield after flash-chromatography (EtOAc). ¹H NMR (CDCl₃) δ 8.27 (d, *J* = 8.7 Hz, 2H), 7.38 (d, *J* = 8.7 Hz, 2H), 5.01–4.95 (m, 1H), 4.70 (s, 2H), 3.91–3.76 (m, 12H).

(1*S*,2*R*)-[1-Benzyl-2-hydroxy-3-(isobutyl(4-methoxybenzenesulfonyl)amino)propyl]carbamic acid (1*S*)-3,5-Dioxacyclooctan-1-yl ester (3a). A solution of **27** (25 mg, 0.05 mmol) in a mixture of 30% trifluoroacetic acid in CH₂Cl₂ (5 mL) was stirred at 23 °C for 40 min and then the solvent was removed under reduced pressure. Compound **28** thus obtained was dissolved in CH₂Cl₂ (4 mL) and a solution of **25a** (16 mg, 0.05 mmol) in THF (2 mL) were added followed by diisopropylethylamine. After 48 h, the organic phase was washed with water, dried (Na₂SO₄), and

evaporated. The residue was purified by flash-chromatography eluting with a 1:4 mixture of EtOAc and hexane to afford **3a** in 63% yield after flash-chromatography (1:4 EtOAc/CHCl₃) as a foam: $[\alpha]_D^{20} + 8.6$ (c 1.1, CHCl₃). ¹H NMR (CDCl₃) δ 7.70 (d, *J* = 9.0 Hz, 2H), 7.31–7.21 (m, 5H), 6.97 (d, *J* = 9.0 Hz, 2H), 4.83–4.78 (m, 2H), 4.65–4.59 (m, 2H), 3.87 (s, 3H), 3.83–3.81 (m, 3H), 3.68 (dd, *J* = 4.9, 12.1 Hz, 1H), 3.55–3.48 (m, 2H), 3.14–2.90 (m, 5H), 2.78 (dd, *J* = 6.8, 12.6 Hz, 1H), 1.85–1.80 (m, 5H), 0.90 (d, *J* = 6.3 Hz, 3H), 0.85 (d, *J* = 6.3 Hz, 3H). ¹³C NMR (CDCl₃) δ 163.0, 153.4, 137.6, 129.8, 129.6, 129.5, 128.4, 126.5, 114.3, 95.7, 73.9, 72.6, 69.2, 68.6, 58.7, 55.6, 55.0, 53.7, 35.4, 29.2, 27.2, 26.1, 20.1, 19.8. HRMS-ESI (*m/z*): (M + Na)⁺ calcd for C₂₈H₄₀N₂NaO₈S, 587.2403; found, 587.2380.

(1S,2R)-[1-Benzyl-2-hydroxy-3-[isobutyl(4-methoxybenzenesulfonyl)amino]propyl]carbamic Acid (1S)-3,5-Dioxacycloheptan-1-yl Ester (3b). The title compound was obtained from **27** and **25b** as described for **3a** in 69% yield after flash-chromatography (1:4 EtOAc/CHCl₃) as an amorphous solid: $[\alpha]_D^{20} + 10.5$ (c 1.2, CHCl₃). ¹H NMR (CDCl₃) δ 7.70 (d, *J* = 8.7 Hz, 2H), 7.31–7.19 (m, 5H), 6.97 (d, *J* = 8.7 Hz, 2H), 4.93 (d, *J* = 8.4 Hz, 1H), 4.77–4.71 (m, 3H), 3.87 (s, 3H), 3.81–3.69 (m, 6H), 3.09–2.90 (m, 5H), 2.77 (dd, *J* = 6.9, 13.2 Hz, 1H), 1.98–1.95 (m, 1H), 1.85–1.76 (m, 2H), 0.90 (d, *J* = 6.9 Hz, 3H), 0.85 (d, *J* = 6.3 Hz, 3H). ¹³C NMR (CDCl₃) δ 162.9, 155.5, 137.5, 129.7, 129.5, 129.4, 128.4, 126.5, 114.3, 94.9, 72.5, 71.9, 68.8, 62.3, 58.9, 55.6, 55.2, 53.7, 35.3, 27.3, 20.2, 19.9. HRMS-ESI (*m/z*): (M + Na)⁺ calcd for C₂₇H₃₈N₂NaO₈S, 573.2247; found, 573.2260.

(1S,2R)-[1-Benzyl-2-hydroxy-3-[isobutyl(4-methoxybenzenesulfonyl)amino]propyl]carbamic Acid (1R)-3,5-Dioxacyclooctan-1-yl Ester (3c). The title compound was obtained from **27** and **25c** as described for **3a** in 50% yield after flash-chromatography (1:4 EtOAc/CHCl₃) as an amorphous solid $[\alpha]_D^{20} + 9.8$ (c 1.1, CHCl₃). ¹H NMR (CDCl₃) δ 7.70 (d, *J* = 8.7 Hz, 2H), 7.31–7.21 (m, 5H), 6.97 (d, *J* = 8.7 Hz, 2H), 4.80–4.79 (m, 2H), 4.65–4.61 (m, 2H), 3.87 (s, 3H), 3.82–3.80 (m, 2H), 3.71–3.62 (m, 2H), 3.56–3.48 (m, 2H), 3.12–2.85 (m, 5H), 2.77 (dd, *J* = 6.3, 13.2 Hz, 1H), 1.83–1.74 (m, 4H), 1.71–1.66 (m, 1H), 0.91 (d, *J* = 6.6 Hz, 3H), 0.86 (d, *J* = 6.6 Hz, 3H). HRMS-ESI (*m/z*): (M + Na)⁺ calcd for C₂₈H₄₀N₂NaO₈S, 587.2403; found, 587.2405.

(1S,2R)-[1-Benzyl-2-hydroxy-3-[isobutyl(4-methoxybenzenesulfonyl)amino]propyl]carbamic Acid (1R)-3,5-Dioxacycloheptan-1-yl Ester (3d). The title compound was obtained from **27** and **25d** as described for **3a** in 59% yield after flash-chromatography (1:4 EtOAc/CHCl₃) as a foam: $[\alpha]_D^{20} + 15.9$ (c 0.6, CHCl₃). ¹H NMR (CDCl₃) δ 7.71 (d, *J* = 9.0 Hz, 2H), 7.30–7.18 (m, 5H), 6.98 (d, *J* = 9.0 Hz, 2H), 4.88 (d, *J* = 8.7 Hz, 1H), 4.77–4.71 (m, 3H), 3.87 (s, 3H), 3.81–3.61 (m, 6H), 3.18–3.07 (m, 2H), 3.04–2.92 (m, 2H), 2.86–2.74 (m, 2H), 1.90–1.77 (m, 3H), 0.92 (d, *J* = 6.3 Hz, 3H), 0.86 (d, *J* = 6.3 Hz, 3H). ¹³C NMR (CDCl₃) δ 162.8, 155.5, 137.6, 129.7, 129.5, 129.4, 128.4, 126.4, 114.3, 94.8, 72.6, 71.9, 68.6, 62.3, 58.8, 55.6, 55.1, 53.8, 35.8, 35.2, 27.3, 20.2, 19.9. HRMS-ESI (*m/z*): (M + Na)⁺ calcd for C₂₇H₃₈N₂NaO₈S, 573.2247; found, 573.2254.

(1S,2R)-[1-Benzyl-2-hydroxy-3-[isobutyl(4-methoxybenzenesulfonyl)amino]propyl]carbamic Acid (R)-Oxepan-3-yl Ester (3e). The title compound was obtained from **27** and **25e** as described for **3a** in 72% yield after flash-chromatography (1:2 EtOAc/hex) as an amorphous solid. ¹H NMR (CDCl₃) δ 7.70 (d, 8.8 Hz, 2H), 7.30–7.19 (m, 5H), 6.97 (d, *J* = 8.8 Hz, 2H), 4.81 (d, *J* = 8.2 Hz, 1H), 4.77–4.74 (m, 1H), 3.87 (s, 3H), 3.81 (m, 3H), 3.70–3.69 (m, 2H), 3.61–3.57 (m, 1H), 3.12 (dd, *J* = 8.2, 14.7 Hz, 1H), 3.05–3.84 (m, 4H), 2.77 (dd, *J* = 6.6, 13.2 Hz, 1H), 1.86–1.60 (m, 6H), 1.49–1.41 (m, 1H), 0.91 (d, *J* = 6.7 Hz, 3H), 0.86 (d, *J* = 6.7 Hz, 3H). ¹³C NMR (CDCl₃) δ 162.9, 155.8, 137.5, 129.6, 129.5, 129.4, 128.4, 126.4, 114.2, 74.5, 73.6, 72.5, 72.4, 58.7, 55.5, 54.8, 53.7, 35.6, 31.9, 30.9, 27.1, 21.0, 20.0, 19.8. HRMS-ESI (*m/z*): (M + Na)⁺ calcd for C₂₈H₄₀N₂NaO₈S, 571.2454; found, 571.2458.

(1S,2R)-[1-Benzyl-2-hydroxy-3-[isobutyl(4-methoxybenzenesulfonyl)amino]propyl]carbamic Acid (S)-oxepan-4-yl ester (3f). The title compound was obtained from **27** and **25f** as described for **3a** in 68% yield after flash-chromatography (1:2 EtOAc/hex) as an amorphous solid. ¹H NMR (CDCl₃) δ 7.71 (d, *J* = 8.8 Hz, 2H), 7.29–7.21 (m, 5H), 6.98 (d, *J* = 8.8 Hz, 2H), 4.78–4.76 (m, 2H), 3.94–3.81 (m, 5H), 3.71–3.60 (m, 3H), 3.56–3.50 (m, 1H), 3.12 (dd, *J* = 8.0, 15.2 Hz, 1H), 3.04–2.86 (m, 4H), 2.79 (dd, *J* = 6.4, 13.1 Hz, 1H), 1.94–1.64 (m, 7H), 0.91 (d, *J* = 6.5 Hz, 3H), 0.86 (d, *J* = 6.5 Hz, 3H). HRMS-ESI (*m/z*): (M + Na)⁺ calcd for C₂₈H₄₀N₂NaO₈S, 571.2454; found, 571.2452.

(1S,2R)-[1-Benzyl-2-hydroxy-3-[isobutyl(4-methoxybenzenesulfonyl)amino]propyl]carbamic Acid Cycloheptanyl Ester (3g). The title compound was obtained from **27** and **25g** as described for **3a** in 84% yield after flash-chromatography (1:6 EtOAc/CHCl₃) as an amorphous solid: $[\alpha]_D^{20} + 16.0$ (c 0.9, CHCl₃). ¹H NMR (CDCl₃) δ 7.70 (d, *J* = 8.7 Hz, 2H), 7.31–7.22 (m, 5H), 6.97 (d, *J* = 8.7 Hz, 2H), 4.69–4.68 (m, 2H), 3.87 (s, 3H), 3.82–3.78 (m, 2H), 3.05–2.77 (m, 6H), 1.83–1.73 (m, 4H), 1.60–1.45 (m, 8H), 1.22–1.20 (m, 1H), 0.90 (d, *J* = 6.3 Hz, 3H), 0.86 (d, *J* = 6.3 Hz, 3H). HRMS-ESI (*m/z*): (M + Na)⁺ calcd for C₂₉H₄₂N₂NaO₈S, 569.2661; found, 569.2663.

(1S,2R)-[1-Benzyl-2-hydroxy-3-[isobutyl(4-methoxybenzenesulfonyl)amino]propyl]carbamic Acid 1,3-Dioxan-5-yl Ester (3h). The title compound was obtained from **25h** and **27** as described for **3a** in 67% yield after flash-chromatography (1:6 EtOAc/CHCl₃): $[\alpha]_D^{20} + 7.9$ (12.3 mg/mL, CH₂Cl₂). ¹H NMR (CDCl₃) δ 7.71 (d, *J* = 9.3 Hz, 2H), 7.32–7.22 (m, 5H), 6.98 (d, *J* = 9.3 Hz, 2H), 5.06 (d, *J* = 8.4 Hz, 1H), 4.92 (d, *J* = 6.2 Hz, 1H), 4.75 (d, *J* = 6.2 Hz, 1H), 4.51–4.49 (m, 1H), 3.95–3.74 (m, 9H), 3.14 (dd, *J* = 8.1, 15.0 Hz, 1H), 3.06–2.84 (m, 4H), 2.77 (dd, *J* = 6.7, 13.3 Hz, 1H), 1.86–1.77 (m, 1H), 0.92 (d, *J* = 6.6 Hz, 3H), 0.87 (d, *J* = 6.6 Hz, 3H). ¹³C NMR (CDCl₃) δ 162.9, 155.4, 137.3, 129.7, 129.6, 129.5, 128.5, 126.5, 114.3, 93.6, 72.3, 68.7, 66.3, 58.8, 55.6, 55.2, 53.8, 35.7, 27.3, 20.2, 19.9. HRMS-ESI (*m/z*): (M + Na)⁺ calcd for C₂₈H₃₈N₂NaO₈S, 559.2090; found, 559.2094.

(1S,2R)-[1-Benzyl-2-hydroxy-3-[isobutyl(4-methoxybenzenesulfonyl)amino]propyl]carbamic Acid 3,6,9-Trioxacyclodecan-1-yl Ester (3i). The title compound was obtained from **25i** and **27** as described for **3a** in 37% yield after flash-chromatography (1:1 EtOAc/CHCl₃) as a white solid: mp 60–62 °C; $[\alpha]_D^{20} + 6.2$ (c 0.3, CHCl₃). ¹H NMR (CDCl₃) δ 7.69 (d, *J* = 8.7 Hz, 2H), 7.33–7.18 (m, 5H), 6.96 (d, *J* = 8.7 Hz, 2H), 5.33 (d, *J* = 8.1 Hz, 1H), 4.84–4.82 (m, 1H), 3.86 (s, 3H), 3.79–3.75 (m, 2H), 3.68–3.55 (m, 12H), 3.07–2.78 (m, 6H), 1.84–1.81 (m, 1H), 0.89 (d, *J* = 7.2 Hz, 3H), 0.85 (d, *J* = 7.2 Hz, 3H). HRMS-ESI (*m/z*): (M + Na)⁺ calcd for C₃₀H₄₂N₂NaO₈S, 617.2509; found, 617.2501.

(1S,2R)-[1-Benzyl-2-hydroxy-3-[isobutyl(4-methoxybenzenesulfonyl)amino]propyl]carbamic Acid 3,6,9,12-Tetraoxacyclotridecan-1-yl Ester (3j). The title compound was obtained from **27** and **25j** as described for **3a** in 30% yield after flash-chromatography (EtOAc) as a foam: $[\alpha]_D^{20} + 17.0$ (c 0.9, CHCl₃). ¹H NMR (CDCl₃) δ 7.70 (d, *J* = 9.0 Hz, 2H), 7.29–7.19 (m, 5H), 6.97 (d, *J* = 9.0 Hz, 2H), 4.96 (d, *J* = 8.0 Hz, 1H), 4.85–4.83 (m, 1H), 3.87 (s, 3H), 3.83–3.81 (m, 2H), 3.80–3.60 (m, 15H), 3.52 (dd, *J* = 3.5, 9.5 Hz, 1H), 3.13 (dd, *J* = 9.0, 15.5 Hz, 1H), 3.02–2.86 (m, 4H), 2.77 (dd, *J* = 6.5, 13.5 Hz, 1H), 1.83–1.76 (m, 1H), 0.90 (d, *J* = 6.5 Hz, 3H), 0.85 (d, *J* = 6.5 Hz, 3H). ¹³C NMR (CDCl₃) (500 MHz) δ 163.0, 155.4, 137.6, 129.7, 129.6, 129.5, 128.5, 126.5, 114.4, 72.4, 71.7, 70.2, 70.1, 69.9, 67.8, 58.7, 55.6, 55.1, 53.7, 35.5, 27.3, 20.2, 19.9. HRMS-ESI (*m/z*): (M + Na)⁺ calcd for C₃₁H₄₄N₂NaO₁₀S, 661.2771; found, 661.2788.

(1S,2R)-[1-Benzyl-2-hydroxy-3-[isobutyl(4-methoxybenzenesulfonyl)amino]propyl]carbamic Acid 3,6,8,11-Tetraoxacyclododecan-1-yl Ester (3k). The title compound was obtained from **27** and **25k** as described for **3a** in 47% yield after flash-chromatography (EtOAc) as a foam: $[\alpha]_D^{20} + 6.5$ (c 0.5, CHCl₃). ¹H NMR (CDCl₃) δ 7.70 (d, *J* = 8.7 Hz, 2H), 7.30–7.18 (m, 5H), 6.97 (d, *J* = 8.7 Hz, 2H), 4.92 (d, *J* = 8.1 Hz, 1H), 4.81–4.76 (m, 1H), 4.66 (s, 2H), 3.87 (s, 3H), 3.78–3.44 (m, 14H), 3.13 (dd, *J* =

8.4, 15.3 Hz, 1H), 3.06–2.82 (m, 4H), 2.75 (dd, $J = 6.9, 13.5$ Hz, 1H), 1.83–1.74 (m, 1H), 0.90 (d, $J = 6.6$ Hz, 3H), 0.85 (d, $J = 6.3$ Hz, 3H). ^{13}C NMR (CDCl_3) δ 163.0, 155.6, 137.5, 129.8, 129.6, 129.5, 128.5, 126.5, 114.4, 94.7, 72.4, 71.5, 69.7, 64.9, 64.5, 58.8, 55.7, 55.1, 53.8, 35.6, 27.3, 20.2, 19.9. HRMS-ESI (m/z): ($M + \text{Na}$) $^+$ calcd for $\text{C}_{30}\text{H}_{44}\text{N}_2\text{NaO}_{10}\text{S}$, 647.2615; found, 647.2590.

(1S,2R)-[1-Benzyl-2-hydroxy-3-[isobutyl(4-methoxybenzenesulfonyl)amino]propyl]carbamic Acid 3,9-Dioxo-6-thiacyclodecan-1-yl 6,6-Dioxide Ester (3l). The title compound was obtained from 27 and 25l as described for 3a in 36% yield after flash-chromatography (1:1 EtOAc/ CHCl_3) as an amorphous solid: $[\alpha]_{\text{D}}^{20} +5.5$ (c 0.7, CHCl_3). ^1H NMR (CDCl_3) δ 7.70 (d, $J = 9.0$ Hz, 2H), 7.31–7.20 (m, 5H), 6.98 (d, $J = 9.0$ Hz, 2H), 4.97 (d, $J = 8.4$ Hz, 1H), 4.85 (t, $J = 4.5$ Hz, 1H), 4.01–3.96 (m, 4H), 3.88 (s, 3H), 3.85–3.83 (m, 2H), 3.71–3.69 (m, 1H), 3.61 (dd, $J = 3.9, 9.3$ Hz, 1H), 3.54–3.47 (m, 2H), 3.61–3.27 (m, 4H), 3.13 (dd, $J = 8.4, 15.0$ Hz, 1H), 3.00–2.82 (m, 4H), 2.75 (dd, $J = 6.6, 13.5$ Hz, 1H), 1.83–1.75 (m, 1H), 0.91 (d, $J = 6.6$ Hz, 3H), 0.86 (d, $J = 6.3$ Hz, 3H). ^{13}C NMR (CDCl_3) δ 163.0, 155.1, 137.4, 131.1, 129.6, 129.4, 128.4, 126.5, 114.3, 72.4, 70.2, 66.0, 64.6, 58.8, 55.7, 55.1, 53.7, 52.2, 35.4, 27.3, 20.2, 19.9. HRMS-ESI (m/z): ($M + \text{Na}$) $^+$ calcd for $\text{C}_{29}\text{H}_{42}\text{N}_2\text{NaO}_{10}\text{S}_2$, 665.2179; found, 665.2191.

***N*-(*tert*-Butoxycarbonyl)-9-(4-nitrophenoxycarbonyloxy)-1,7-dioxo-4-azocyclodecane (29).** The title compound was obtained from 24 as described for 25a in 73% yield after flash-chromatography (1:4 EtOAc/ CHCl_3). ^1H NMR (CDCl_3) δ 8.27 (d, $J = 9.0$ Hz, 2H), 7.37 (d, $J = 9.0$ Hz, 2H), 5.02–4.96 (m, 1H), 3.98–3.76 (m, 8H), 4.52–3.23 (m, 4H), 1.47 (s, 9H).

(1S,2R)-[1-Benzyl-2-hydroxy-3-[isobutyl(4-methoxybenzenesulfonyl)amino]propyl]carbamic Acid *N*-(*tert*-Butoxycarbonyl)-1,7-dioxo-4-azocyclodecan-9-yl Ester (30). The title compound was obtained from 27 and 29 as described for 3a in 74% yield after flash-chromatography (1:1 EtOAc/ CHCl_3) as a white solid: mp 71–73 °C; $[\alpha]_{\text{D}}^{20} +4.7$ (c 1.7, CHCl_3). ^1H NMR (CDCl_3) 7.70 (d, $J = 9.0$ Hz, 2H), 7.30–7.20 (m, 5H), 7.0 (d, $J = 9.0$ Hz, 2H), 4.92–4.90 (m, 1H), 4.81 (t, $J = 4.0$ Hz, 1H), 3.86 (s, 3H), 3.79–3.66 (m, 6H), 3.62–3.57 (m, 2H), 3.49–3.42 (m, 2H), 3.40–3.28 (m, 4H), 3.12 (dd, $J = 7.8, 15.3$ Hz, 1H), 3.01–2.82 (m, 4H), 2.75 (dd, $J = 6.3, 13.2$ Hz, 1H), 1.83–1.74 (m, 1H), 1.44 (s, 9H), 0.90 (d, $J = 6.6$ Hz, 3H), 0.85 (d, $J = 6.6$ Hz, 3H). ^{13}C NMR (CDCl_3) 163.0, 155.6, 155.4, 137.4, 129.7, 129.5, 129.4, 128.4, 126.5, 114.3, 79.9, 72.4, 71.9, 71.0, 68.6, 68.1, 58.7, 55.6, 55.0, 53.7, 50.3, 35.6, 28.5, 27.3, 20.2, 19.9.

(1S,2R)-[1-Benzyl-2-hydroxy-3-[isobutyl(4-methoxybenzenesulfonyl)amino]propyl]carbamic Acid 1,7-Dioxo-4-azocyclodecan-9-yl Ester (31). A solution of 30 (13 mg, 0.02 mmol) in a mixture of 30% trifluoroacetic acid in CH_2Cl_2 (1 mL) was stirred at 23 °C for 30 min and then the solvent was removed under reduced pressure. The residue was dissolved in CH_2Cl_2 , and the organic phase was washed with a saturated solution of NaHCO_3 , dried (Na_2SO_4), and evaporated to afford 11 mg (100%) of 31 as a white solid: mp 65–66 °C; $[\alpha]_{\text{D}}^{20} +13.8$ (c 0.7, CHCl_3). ^1H NMR (CDCl_3) δ 7.70 (d, $J = 8.7$ Hz, 2H), 7.30–7.18 (m, 5H), 6.97 (d, $J = 8.7$ Hz, 2H), 5.20 (d, $J = 8.4$ Hz, 1H), 4.82–4.79 (m, 1H), 3.87 (s, 3H), 3.84–3.80 (m, 2H), 3.75–3.64 (m, 7H), 3.54 (dd, $J = 5.4, 10.2$ Hz, 1H), 3.13 (dd, $J = 8.4, 15.3$ Hz, 1H), 3.04–2.84 (m, 8H), 2.77 (dd, $J = 6.9, 13.5$ Hz, 1H), 2.38 (bs, 1H), 1.85–1.76 (m, 1H), 0.90 (d, $J = 6.3$ Hz, 3H), 0.85 (d, $J = 6.6$ Hz, 3H). ^{13}C NMR (CDCl_3) δ 162.9, 155.3, 137.5, 129.8, 129.5, 129.4, 128.4, 126.4, 114.3, 72.4, 71.8, 68.6, 58.7, 55.6, 55.1, 53.6, 53.4, 48.2, 35.6, 27.2, 20.2, 19.9.

(1S,2R)-[1-Benzyl-2-hydroxy-3-[isobutyl(4-methoxybenzenesulfonyl)amino]propyl]carbamic Acid *N*-Methyl-1,7-dioxo-4-azocyclodecan-9-yl Ester (3m). To a solution of 31 (9.0 mg, 0.015 mmol) in a mixture of 1% acetic acid in methanol (0.5 mL), formaldehyde (37% solution in H_2O , 12 μL , 0.15 mmol), and sodium cyanoborohydride (2.0 mg, 0.03 mmol) were added. After 18 h, a saturated solution of NaHCO_3 was added, the solvent was removed and the aqueous phase was extracted with CH_2Cl_2 . The organic extracts were dried (Na_2SO_4), evaporated, and the residue was purified by flash-chromatography eluting with a 10:1 mixture

of CHCl_3 and MeOH to afford 8.0 mg (87%) of 3m as an amorphous solid: $[\alpha]_{\text{D}}^{20} +8.1$ (c 0.6, CHCl_3). ^1H NMR (CDCl_3) δ 7.70 (d, $J = 8.7$ Hz, 2H), 7.3–7.18 (m, 5H), 6.98 (d, $J = 8.7$ Hz, 2H), 4.99 (d, $J = 8.1$ Hz, 1H), 4.80–4.77 (m, 1H), 3.87 (s, 3H), 3.83–3.74 (m, 4H), 3.70–3.56 (m, 6H), 3.14 (dd, $J = 8.1, 14.7$ Hz, 1H), 3.02–2.69 (m, 9H), 2.40 (s, 3H), 1.83–1.74 (m, 1H), 0.90 (d, $J = 6.3$ Hz, 3H), 0.85 (d, $J = 6.6$ Hz, 3H). ^{13}C NMR (CDCl_3) δ 162.9, 155.5, 137.4, 129.9, 129.4 ($\times 2$), 128.4, 126.4, 114.3, 77.2, 72.3, 69.6, 67.6, 59.0, 55.6, 55.1, 53.6, 44.0, 35.6, 29.7, 27.2, 20.2, 19.9. HRMS-ESI (m/z): ($M + \text{Na}$) $^+$ calcd for $\text{C}_{30}\text{H}_{46}\text{N}_2\text{O}_8\text{S}$, 608.3006; found, 608.3009.

Determination of X-ray Structure of 3d-Bound HIV Protease. The HIV-1 protease construct with the substitutions Q7K, L33I, L63I, C67A, and C95A to optimize protein stability³³ was expressed and purified as described.³⁴ Crystals were grown by the hanging drop vapor diffusion method using a 1:15 molar ratio of protease at 2.0 mg/mL and inhibitor dissolved in dimethylsulfoxide. The reservoir contained 0.1 M sodium acetate buffer (pH = 4.2) and 1.2 M NaCl, 10% DMSO. Crystals were transferred into a cryoprotectant solution containing the reservoir solution and 20–30% (v/v) glycerol, mounted on a nylon loop and flash-frozen in liquid nitrogen. X-ray diffraction data were collected on the SER-CAT beamline of the Advanced Photon Source, Argonne National Laboratory. Diffraction data were processed using HKL2000,³⁵ resulting in an R_{merge} value of 8.0% (41.1%) for 110362 unique reflections between 50 and 1.00 Å resolution with a completeness of 88.4% (52.6%), where the values in parentheses are for the final highest resolution shell. Data were reduced in space group $P2_12_12$ with unit cell dimensions of $a = 57.96$ Å, $b = 86.41$ Å, $c = 46.03$ Å with one dimer in the asymmetric unit. The structure was solved by molecular replacement using the CPP4i suite of programs,^{36,37} with the structure of the D30N mutant of HIV protease in complex with GRL-98065 (2QCD)³⁴ as the starting model. The structure was refined using SHELX97³⁸ and refitted manually using the molecular graphics programs O³⁹ and COOT.⁴⁰ Alternate conformations were modeled for the protease residues when obvious in the electron density maps. Anisotropic atomic displacement parameters (B -factors) were refined for all atoms including solvent molecules. Hydrogen atoms were added at the final stages of the refinement. The identity of ions and other solvent molecules from the crystallization conditions was deduced from the shape and peak height of the $2F_o - F_c$ and $F_o - F_c$ electron density, the hydrogen bond interactions, and interatomic distances. The solvent structure was refined with two sodium ions, three chloride ions, and 219 water molecules including partial occupancy sites. The final R_{work} was 14.7% and R_{free} was 17.5% for all data between 10 and 1.00 Å resolution. The rmsd values from ideal bonds and angle distances were 0.017 Å and 0.034 Å, respectively. The average B -factor was 11.4 and 16.5 Å² for protease main chain and side chain atoms, respectively, 12.9 Å² for inhibitor atoms, and 22.6 Å² for solvent atoms. The X-ray crystal structure of the 3d-bound HIV-1 protease has been deposited in the Protein Data Bank (PDB)⁴¹ with accession code 3DJK.

Acknowledgment. This research was supported by grants from the National Institutes of Health (GM53386, A.K.G., and GM62920, I.W.). This work was also supported by the Intramural Research Program of the Center for Cancer Research, National Cancer Institute, National Institutes of Health and in part by a Grant-in-aid for Scientific Research (Priority Areas) from the Ministry of Education, Culture, Sports, Science, and Technology of Japan (Monbu Kagakusho), a Grant for Promotion of AIDS Research from the Ministry of Health, Welfare, and Labor of Japan (Kosei Rohdoshō: H15-AIDS-001), and the Grant to the Cooperative Research Project on Clinical and Epidemiological Studies of Emerging and Re-emerging Infectious Diseases (Renkei Jigyō: no. 78, Kumamoto University) of Monbu-Kagakusho. The work was also supported in part by the Georgia State University Molecular Basis of Disease

Program, the Georgia Research Alliance, the Georgia Cancer Coalition. We thank the staff at the SER-CAT beamline at the Advanced Photon Source, Argonne National Laboratory, for assistance during X-ray data collection. Use of the Advanced Photon Source was supported by the U.S. Department of Energy, Office of Science, Office of Basic Energy Sciences, under contract no. DE-AC02-06CH11357. We also thank Sofiya Leshchenko-Yashchuk for her assistance in HIV-1 protease inhibitory assay.

Supporting Information Available: HPLC and HRMS data of inhibitors **3a–m**; crystallographic data collection and refinement statistics. This material is available free of charge via the Internet at <http://pubs.acs.org>.

References

- Sepkowitz, K. A. AIDS—The first 20 years. *Engl. J. Med.* **2001**, *344*, 1764–1772.
- Waters, L.; Nelson, M. Why do patients fail HIV therapy? *Int. J. Clin. Pract.* **2007**, *61*, 983–990.
- Pillay, D.; Bhaskaran, K.; Jurriaans, S.; Prins, M.; Masquelier, B.; Dabis, F.; Gifford, R.; Nielsen, C.; Pedersen, C.; Balotta, C.; Rezza, G.; Ortiz, M.; de Mendoza, C.; Kucherer, C.; Poggensee, G.; Gill, J.; Porter, K. The impact of transmitted drug resistance on the natural history of HIV infection and response to first-line therapy. *AIDS* **2006**, *20*, 21–28.
- Grabar, S.; Pradier, C.; Le Corfec, E.; Lancar, R.; Allavena, C.; Bentata, M.; Berlureau, P.; Dupont, C.; Fabbro-Peray, P.; Poizat-Martin, I.; Costagliola, D. Factors associated with clinical and virological failure in patients receiving a triple therapy including a protease inhibitor. *AIDS* **2000**, *14*, 141–149.
- Wainberg, M. A.; Friedland, G. Public health implications of antiretroviral therapy and HIV drug resistance. *J. Am. Med. Assoc.* **1998**, *279*, 1977–1983.
- Harrigan, P. R.; Hogg, R. S.; Dong, W. W.; Yip, B.; Wynhoven, B.; Woodward, J.; Brumme, C. J.; Brumme, Z. L.; Mo, T.; Alexander, C. S.; Montaner, J. S. Predictors of HIV drug-resistance mutations in a large antiretroviral naive cohort initiating triple antiretroviral therapy. *J. Infect. Dis.* **2005**, *191*, 339–347.
- Hertogs, K.; Bloor, S.; Kemp, S. D.; Van den Eynde, C.; Alcorn, T. M.; Pauwels, R.; Van Houtte, M.; Staszewski, S.; Miller, V.; Larder, B. A Phenotypic and genotypic analysis of clinical HIV-1 isolates reveals extensive protease inhibitor cross-resistance: a survey of over 6000 samples. *AIDS* **2000**, *14*, 1203–1210.
- Yerly, S.; Kaiser, L.; Race, E.; Bru, J. P.; Clavel, F.; Perrin, L. Transmission of antiretroviral drug resistant HIV-1 variants. *Lancet* **1999**, *354*, 729–733.
- On June 23, 2006, FDA approved new HIV treatment for patients who do not respond to existing drugs. Please see: <http://www.fda.gov/bbs/topics/NEWS/2006/NEW01395.html>.
- Ghosh, A. K.; Kincaid, J. F.; Cho, W.; Walters, D. E.; Krishnan, K.; Hussain, K. A.; Koo, Y.; Cho, H.; Rudall, C.; Holland, L.; Bufnold, J. Potent HIV protease inhibitors incorporating high-affinity P2-ligands and (R)-(hydroxyethylamino)sulfonamide isostere. *Bioorg. Med. Chem. Lett.* **1998**, *8*, 687–690.
- Koh, Y.; Nakata, H.; Maeda, K.; Ogata, H.; Bilcer, G.; Devasamudram, T.; Kincaid, J. F.; Boross, P.; Wang, Y.-F.; Tse, Y.; Volarath, P.; Gaddis, L.; Harrison, R. W.; Weber, I. T.; Ghosh, A. K.; Mitsuya, H. A novel bis-tetrahydrofuranylurethane-containing non-peptide protease inhibitor (PI) UIC-94017 (TMC-114) potent against multi-PI-resistant HIV in vitro. *Antimicrob. Agents Chemother.* **2003**, *47*, 3123–3129.
- Surleraux, D. L. N. G.; Tahri, A.; Verschuere, W. G.; Pille, G. M. E.; de Kock, H. A.; Jonckers, T. H. M.; Peeters, A.; De Meyer, S.; Azijn, H.; Pauwels, R.; de Bethune, M.-P.; King, N. M.; Prabu-Jeyabalan, M.; Schiffer, C. A.; Wigerinck, P. B. T. P. Discovery and selection of TMC114, a next generation of HIV-1 protease inhibitor. *J. Med. Chem.* **2005**, *48*, 1813–1822.
- Yoshimura, K.; Kato, R.; Kavlick, M. F.; Nguyen, A.; Maroun, V.; Maeda, K.; Hussain, K. A.; Ghosh, A. K.; Gulnik, S. V.; Erickson, J. W.; Mitsuya, H. A potent human immunodeficiency virus type 1 protease inhibitor, UIC-94003 (TMC-126), and selection of a novel (A28S) mutation in the protease active site. *J. Virol.* **2002**, *76*, 1349–1358.
- (a) Kohl, Y.; Maeda, K.; Ogata, H.; Bilcer, G.; Devasamudram, T.; Kincaid, J. F.; Boross, P.; Wang, Y.-F.; Tse, Y.; Volarath, P.; Gaddis, L.; Louis, J. M.; Harrison, R. W.; Weber, I. T.; Ghosh, A. K.; Mitsuya, H. Novel bis-tetrahydrofuranyl-urethane-containing nonpeptide protease inhibitor (PI) UIC-94017 (TMC114) potent against multi-PI-resistant human immunodeficiency virus in vitro. *Antimicrob. Agents Chemother.* **2003**, *47*, 3123–3129. (b) Ghosh, A. K.; Pretzer, E.; Cho, H.; Hussain, K. A.; Duzgunes, N. Antiviral activity of UIC-PI, a novel inhibitor of the human immunodeficiency virus type 1 protease. *Antiviral Res.* **2002**, *54*, 29–36.
- Tie, Y.; Boross, P. I.; Wang, Y.-F.; Gaddis, L.; Hussain, A. K.; Leshchenko, S.; Ghosh, A. K.; Louis, J. M.; Harrison, R. W.; Weber, I. T. High-resolution crystal structures of HIV-1 protease with a potent non-peptide inhibitor (UIC-94017) active against multidrug-resistant clinical strains. *J. Mol. Biol.* **2004**, *338*, 341–352.
- Hong, L.; Zhang, X. C.; Hartsuck, J. A.; Tang, J. Crystal structure of an in vivo HIV-1 protease mutant in complex with saquinavir: Insights into the mechanisms of drug resistance. *Protein Sci.* **2000**, *9*, 1989–1994.
- Laco, G. S.; Schaik-Hühi, C.; Lubkowski, J.; Morris, G.; Zdanov, A.; Olson, A.; Elder, J. H.; Wlodawer, A.; Gustchina, A. Crystal Structures of the Inactive D30N Mutant of Feline Immunodeficiency Virus Protease Complexed with a Substrate and an Inhibitor. *Biochemistry* **1997**, *36*, 10696–10708.
- Winitz, M.; Bloch-Frankenthal, L.; Izumiya, N.; Birnbaum, S. M.; Baker, C. G.; Greenstein, J. P. Studies on Diastereoisomeric α -Amino Acids and Corresponding α -Hydroxy Acids. VII. *J. Am. Chem. Soc.* **1956**, *78*, 2423–2430.
- Soai, K.; Ookawa, A. Mixed solvents containing methanol as useful reaction media for unique chemoselective reductions with lithium borohydride. *J. Org. Chem.* **1986**, *51*, 4000–4005.
- Gmeiner, P.; Junge, D. Regioselective transformation of malic acid: a practical method for the construction of enantiomerically pure indolizidines. *J. Org. Chem.* **1995**, *60*, 3910–3915.
- Le Merrer, Y.; Gauzy, L.; Gravier-Pelletier, C.; Depeyaz, J.-C. Synthesis of C₂-symmetric guanidino-sugars as potent inhibitors of glycosidases. *Bioorg. Med. Chem.* **2000**, *8*, 307–320.
- Pospisil, J.; Markó, I. E. Total synthesis of (R)-(+)-goniothalamin and (R)-(+)-goniothalamin oxide: first application of the sulfoxide-modified Julia olefination in total synthesis. *Tetrahedron Lett.* **2007**, *47*, 5933–5937.
- Lu, C.-D.; Zakarian, A. Studies toward the synthesis of pinnatoxins: The B,C,D-dispiroketal fragment. *Org. Lett.* **2007**, *9*, 3161–3163.
- Kasireddy, K.; Ahmad, M. U.; Ali, S. M.; Ahmad, I. Synthesis of novel cationic cardiolipin analogues for the optimal delivery of therapeutic agents. *Tetrahedron Lett.* **2004**, *45*, 2743–2746.
- Calverley, M. J.; Dale, J. 1,4,7-Trioxa-10-azacyclododecane and some N-substituted derivatives; synthesis and cation complexing. *Acta Chem. Scand.* **1982**, *B36*, 241–247.
- Sakamoto, H.; Kimura, K.; Koseki, Y.; Matsuo, M.; Shono, T. Lipophilic bis(monooxa crown ether) derivatives: synthesis and cation-complexing properties. *J. Org. Chem.* **1986**, *51*, 4974–4979.
- Ghosh, A. K.; Fidanze, S. Transition-state mimetics for HIV protease inhibitors: stereocontrolled synthesis of hydroxyethylene and hydroxyethylamine isosteres by ester-derived titanium enolate *syn*- and *anti*-aldol reactions. *J. Org. Chem.* **1998**, *63*, 6146–6152.
- Toth, M. V.; Marshall, G. R. A simple, continuous fluorometric assay for HIV protease. *Int. J. Pep. Protein Res.* **1990**, *36*, 544–550.
- Gustchina, A.; Sansom, C.; Prevost, M.; Richelle, J.; Wodak, S.; Wlodawer, A.; Weber, I. Energy calculations and analysis of HIV-1 protease-inhibitor crystal structures. *Protein Eng.* **1994**, *7*, 309–317.
- Tie, Y.; Boross, P. I.; Wang, Y. F.; Gaddis, L.; Liu, F.; Chen, X.; Tozser, J.; Harrison, R. W.; Weber, I. T. Molecular basis for substrate recognition and drug resistance from 1.1 to 1.6 Angstroms resolution crystal structures of HIV-1 protease mutants with substrate analogs. *FEBS J.* **2005**, *272*, 5265–5277.
- Wang, Y. F.; Tse, Y.; Boross, P. I.; Tozser, J.; Ghosh, A. K.; Harrison, R. W.; Weber, I. T. Potent new antiviral compound shows similar inhibition and structural interactions with drug resistant mutants and wild type HIV-1 protease. *J. Med. Chem.* **2007**, *50*, 4509–4515.
- Hronowski, L. J. J.; Szarek, W. A.; Hay, G. W.; Krebs, A.; Depew, W. T. Synthesis and characterization of 1-O- β -lactosyl-(R,S)-glycerols and 1,3-di-O- β -lactosylglycerol. *Carbohydr. Res.* **1989**, *190*, 203–218.
- Louis, J. M.; Clore, G. M.; Gronenborn, A. M. Autoprocessing of HIV-1 protease is tightly coupled to protein folding. *Nat. Struct. Biol.* **1999**, *6*, 868–875.
- Mahalingam, B.; Louis, J. M.; Hung, J.; Harrison, R. W.; Weber, I. T. Structural implications of drug resistant mutants of HIV-1 protease: High resolution crystal structures of the mutant protease/substrate analog complexes. *Proteins* **2001**, *43*, 455–464.
- Otwinski, Z.; Minor, W. Processing of X-ray diffraction data in oscillation mode. *Methods Enzymol.* **1997**, *276*, 307–326.
- Collaborative Computational Project, Number 4. The CCP4 Suite: Programs for Protein Crystallography. *Acta Crystallogr., Sect. D: Biol. Crystallogr.* **1994**, *50*, 760–763.

- (37) Potterton, E.; Briggs, P.; Turkenburg, M.; Dodson, E. A graphical user interface to the CCP4 program suite. *Acta Crystallogr., Sect. D: Biol. Crystallogr.* **2003**, *59*, 1131–1137.
- (38) Sheldrick, G. M.; Schneider, T. R. SHELXL: High resolution refinement. *Methods Enzymol.* **1997**, *277*, 319–343.
- (39) Jones, T. A.; Zou, J. Y.; Cowan, S. W.; Kjeldgaard, M. Improved methods for building protein models in electron density maps and the location of errors in these models. *Acta Crystallogr., Sect. A: Found. Crystallogr.* **1991**, *47*, 110–119.
- (40) Emsley, P.; Cowtan, K. Coot: Model-Building Tools for Molecular Graphics. *Acta Crystallogr., Sect. D: Biol. Crystallogr.* **2004**, *60*, 2126–2132.
- (41) Berman, H. M.; Westbrook, J.; Feng, Z.; Gilliland, G.; Bhat, T. N.; Weissig, H.; Shindyalov, I. N.; Bourne, P. E. The Protein Data Bank. *Nucleic Acids Res.* **2000**, *28*, 235–242.
- (42) (a) Shirasaka, T.; Yarchoan, R.; O'Brien, M. C.; Husson, R. N.; B., D.; Kojima, E.; Broder, S.; Mitsuya, H. Changes in drug sensitivity of human immunodeficiency virus type 1 during therapy with azidothymidine, dideoxycytidine, and dideoxyinosine: An in vitro comparative study. *Proc. Natl. Acad. Sci. U.S.A.* **1993**, *90*, 562–566. (b) Perno, C. F.; Yarchoan, R.; Cooney, D. A.; Hartman, N. R.; Webb, D. S. A.; Hao, Z.; Mitsuya, H.; Johns, D. G.; Broder, S. Replication of HIV in monocytes: Granulocyte-macrophage colony stimulating factor (GM-CSF) potentiates viral production yet enhances the antiviral effect mediated by AZT and other dideoxynucleoside congeners of thymidine. *J. Exp. Med.* **1989**, *169*, 933–951.

JM8004543

Involvement of the Second Extracellular Loop and Transmembrane Residues of CCR5 in Inhibitor Binding and HIV-1 Fusion: Insights into the Mechanism of Allosteric Inhibition

Kenji Maeda¹, Debananda Das¹, Philip D. Yin¹, Kiyoto Tsuchiya¹, Hiromi Ogata-Aoki², Hirotomo Nakata¹, Rachael B. Norman¹, Lauren A. Hackney¹, Yoshikazu Takaoka³ and Hiroaki Mitsuya^{1,2*}

¹Experimental Retrovirology Section, HIV and AIDS Malignancy Branch, National Cancer Institute, National Institutes of Health, Bethesda, MD, USA

²Departments of Hematology and Infectious Diseases, Kumamoto University Graduate School of Medical and Pharmaceutical Sciences, Kumamoto, Japan

³Minase Research Institute, Ono Pharmaceutical Co. Ltd., Osaka, Japan

Received 6 March 2008;
received in revised form
12 June 2008;
accepted 13 June 2008
Available online
20 June 2008

C-C chemokine receptor 5 (CCR5), a member of G-protein-coupled receptors, serves as a coreceptor for human immunodeficiency virus type 1 (HIV-1). In the present study, we examined the interactions between CCR5 and novel CCR5 inhibitors containing the spirodiketopiperazine scaffolds AK530 and AK317, both of which were lodged in the hydrophobic cavity located between the upper transmembrane domain and the second extracellular loop (ECL2) of CCR5. Although substantial differences existed between the two inhibitors—AK530 had 10-fold-greater CCR5-binding affinity ($K_d=1.4$ nM) than AK317 (16.7 nM)—their antiviral potencies were virtually identical ($IC_{50}=2.1$ nM and 1.5 nM, respectively). Molecular dynamics simulations for unbound CCR5 showed hydrogen bond interactions among transmembrane residues Y108, E283, and Y251, which were crucial for HIV-1-gp120/sCD4 complex binding and HIV-1 fusion. Indeed, AK530 and AK317, when bound to CCR5, disrupted these interhelix hydrogen bond interactions, a salient molecular mechanism enabling allosteric inhibition. Mutagenesis and structural analysis showed that ECL2 consists of a part of the hydrophobic cavity for both inhibitors, although AK317 is more tightly engaged with ECL2 than AK530, explaining their similar anti-HIV-1 potencies despite the difference in K_d values. We also found that amino acid residues in the β -hairpin structural motif of ECL2 are critical for HIV-1-elicited fusion and binding of the spirodiketopiperazine-based inhibitors to CCR5. The direct ECL2-engaging property of the inhibitors likely produces an ECL2 conformation, which HIV-1 gp120 cannot bind to, but also prohibits HIV-1 from utilizing the “inhibitor-bound” CCR5 for cellular entry—a mechanism of HIV-1’s resistance to CCR5 inhibitors. The data should not only help delineate the dynamics of CCR5 following inhibitor binding but also aid in designing CCR5 inhibitors that are more potent against HIV-1 and prevent or delay the emergence of resistant HIV-1 variants.

Published by Elsevier Ltd.

Keywords: HIV-1; CCR5 inhibitor; GPCR structure; allosteric inhibition; extracellular loop

Edited by M. F. Summers

*Corresponding author. E-mail address: himitsuya@helix.nih.gov.

Abbreviations used: CCR5, C-C chemokine receptor 5; HIV-1, human immunodeficiency virus type 1; ECL2, second extracellular loop; GPCR, G-protein-coupled seven-transmembrane segment receptor; MVC, maraviroc; APL, aplaviroc; SDP, spirodiketopiperazine; TM1, transmembrane region 1; TM2, transmembrane region 2; TM3, transmembrane region 3; TM4, transmembrane region 4; TM5, transmembrane region 5; TM6, transmembrane region 6; TM7, transmembrane region 7; PHA, phytohemagglutinin; PBM, peripheral blood mononuclear; CHO, Chinese hamster ovary; mAb, monoclonal antibody; FCS, fetal calf serum; PDB, Protein Data Bank.

Introduction

C-C chemokine receptor 5 (CCR5) is a member of G-protein-coupled seven-transmembrane segment receptors (GPCRs), which comprise the largest superfamily of proteins in the body.¹ In 1996, it was revealed that CCR5 represents one of the two essential coreceptors for human immunodeficiency virus type 1 (HIV-1) entry into human CD4⁺ cells, thereby serving as an attractive target for possible intervention for HIV-1 infection using CCR5 as a coreceptor (R5-HIV-1).²⁻⁵ The second extracellular loop (ECL2) of GPCRs is known to play a critical role in ligand binding and ensuing signal transduction. The ECL2 of CCR5 is also thought to play an important role in CCR5 interactions with HIV-1 envelope. To date, scores of newly designed and synthesized CCR5 inhibitors have been reported to be potent against R5-HIV-1,⁶⁻¹⁵ one such inhibitor, maraviroc (MVC),^{11,15} has recently been approved by the US Food and Drug Administration for treatment of HIV-1-infected individuals who do not respond to any existing antiretroviral regimen.

HIV-1 gp120 interacts with CCR5 following its binding to CD4, and such an interaction is thought to involve the V3 region of gp120 and the N-terminus and extracellular loops of CCR5.^{16,17} Recent reports¹⁸⁻²¹ have determined the orientation and location of CCR5 inhibitors within CCR5 and have shown that those inhibitors are all located in a hydrophobic cavity formed by the transmembrane domains of CCR5. In fact, earlier reports demonstrated that mutations in the extracellular loops did not have any effect on the binding of CCR5 inhibitors SCH-C and TAK-779.^{19,22,23} Taking these observations together, the binding sites in CCR5 for CCR5 inhibitors distinctly differ from the binding sites in CCR5 for HIV-1 gp120, strongly suggesting that CCR5 inhibitors block the interactions of CCR5 with HIV-1 gp120 by eliciting allosteric changes in extracellular loop structures.^{9,22,23}

We previously reported a small-molecule CCR5 inhibitor, aplaviroc (APL; 4-[4-[(3R)-1-butyl-3-[(1R)-cyclohexylhydroxymethyl]-2,5-dioxo-1,4,9-triazaspiro [5.5] undec-9-ylmethyl] phenoxy] benzoic acid hydrochloride), which has a high affinity for CCR5 (K_d values of 3 nM) and exerts potent activity against a wide spectrum of R5-HIV-1 isolates, including multidrug-resistant R5-HIV-1 strains.^{14,24} APL significantly reduced viremia in patients with HIV-1

infection, as examined in a phase 2a clinical trial in the United States. However, in phase 2b clinical trials enrolling about 300 patients, four individuals receiving APL developed grade 3 or greater treatment-emergent elevations in ALT; in late 2005, the clinical development of APL was terminated. However, using APL as a specific probe, we further conducted structural analyses of CCR5 inhibitor interactions with CCR5, employing homology modeling, robust structure refinement, and molecular docking based on site-directed-mutagenesis-based saturation binding assay data of CCR5 inhibitors.²²

In the current study, we determined the structural and molecular interactions of two novel CCR5 inhibitors, AK530 [(3S)-1-but-2-yn-1-yl-3-[(1S)-cyclohexyl-hydroxymethyl]-9-(3,5-dimethyl-1-phenyl-1H-pyrazol-4-ylmethyl)-1,4,9-triazaspiro [5.5] undecane-2,5-dione dihydrochloride] and AK317 [4-(4-[(3S)-1-butyl-3-(cyclohexylmethyl)-2,5-dioxo-1,4,9-triazaspiro[5.5] undec-9-yl] methyl) phenoxy] benzoic acid hydrochloride] (Fig. 1), both of which contain a novel spirodiketopiperazine (SDP) scaffold. We found that these two inhibitors lodge in a hydrophobic cavity located between the upper transmembrane domain and the ECL2 of CCR5. We found substantial differences between the two molecules: AK530 had a 10-fold-greater CCR5-binding affinity ($K_d=1.4$ nM) than AK317 ($K_d=16.7$ nM), while their antiviral potencies were virtually identical [$IC_{50}=2.1$ nM (AK530) and 1.5 nM (AK317)]. Modeling analysis showed that AK530 has the least interactions with S180 and K191 of ECL2, with which AK317 has a close association, suggesting that the interaction profile of the inhibitors with ECL2 residues is one of the important determinants of antiviral potency. We also found that the hairpin motif in the N-terminal half of ECL2 is critical for HIV-1-envelope-elicited fusion event. The direct ECL2-engaging property of the inhibitors likely produces an ECL2 conformation, which HIV-1 gp120 cannot bind to, but also prohibits or substantially delays the emergence of HIV-1 that utilizes the "inhibitor-bound" CCR5 for cellular entry—a mechanism of HIV-1's resistance to CCR5 inhibitors. We also carried out molecular dynamics simulations of unbound CCR5 and compared the conformation with inhibitor-bound CCR5. Critical interhelix hydrogen bond interactions and interactions between the helices and the ECL2 seen in the unbound CCR5 were lost when transmembrane helix residues rearranged to

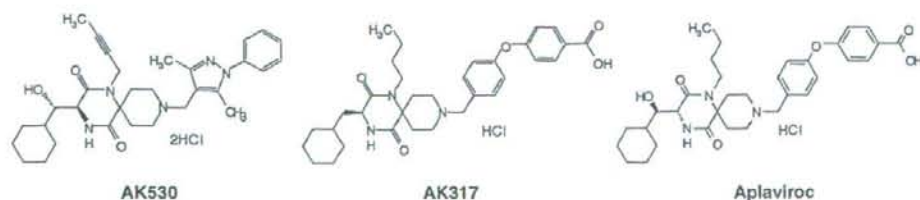


Fig. 1. Structures of small-molecule CCR5 inhibitors AK530, AK317, and APL.

accommodate AK530 and AK317 in the binding pocket. These observations add considerable insights into the mechanism of the allosteric inhibition of CCR5-gp120 interaction by CCR5 inhibitors.

Results

Structural modeling of unliganded human CCR5

It is thought that the ECL2 of human CCR5 (Fig. 2) plays an important role in the binding of CC chemokines to CCR5, as well as in the binding of HIV-1-gp120/CD4 complex to CCR5 in the cellular entry of HIV-1.^{25,26} On the other hand, certain amino acid residue substitutions such as Y108A, Y251A, and E283A, all of which are located in the transmembrane domain (Fig. 2a), significantly reduce both HIV-1-gp120/CD4 complex binding to CCR5 and HIV-1 susceptibility of CCR5-expressing cells, as previously described.²²

In the present study, in an attempt to examine the interplays of ECL2 and selected amino acid residues consisting of the largest hydrophobic cavity within CCR5, which accommodates small-molecule CCR5 inhibitors, we generated a homology model of CCR5, without any ligands bound, using the crystal structure of bovine rhodopsin as template.²⁷ In generating the model, the following structural assignment to CCR5 was made: residues 1 through 26 were assigned to the N-terminus region; residues 27 through 57 were assigned to transmembrane region 1 (TM1); residues 58 through 63 were assigned to the first cytoplasmic region; residues 64 through 93 were assigned to transmembrane region 2 (TM2); residues 94 through 96 were assigned to the first extracellular loop; residues 97 through 130 were assigned to transmembrane region 3 (TM3); residues 131 through 141 were assigned to the second cytoplasmic region; residues 142 through 165 were assigned to transmembrane region 4 (TM4); residues 166 through 190 were assigned to ECL2; residues 191 through 219 were assigned to transmembrane region 5 (TM5); residues 220 through 231 were assigned to the third cytoplasmic region; residues 232 through 259 were assigned to transmembrane region 6 (TM6); residues 260 through 278 were assigned to the third extracellular loop; residues 279 through 300 were assigned to transmembrane region 7 (TM7); residues 303 through 312 were assigned to the helix region (H8) in the cytoplasmic domain; and residues from 313 were assigned to the C-terminus (Fig. 2).

To more effectively sample the conformational space occupied by CCR5, we carried out molecular dynamics simulation for 4800 ps to efficiently explore the conformational space of CCR5. The simulation was carried out in implicit water with a time step of 1 fs, and without any distance cutoffs for nonbonded van der Waals and electrostatic interactions. These stringent conditions added considerably to the overall computation time, but are thought to provide robust results. The conformations at intervals of 50 ps were analyzed. As

expected, there are several hydrogen bonds between nearby residues in the same transmembrane helix that are important for maintaining the helical structure. Examples of such interactions are between W248 and Y251 in TM6, and between E283 and M287 in TM7 (Fig. 3).

We identified a hydrogen bond network involving multiple helices and ECL2: Y108(TM3), E283(TM7), Y251(TM6), and S180(ECL2) (Fig. 3). These hydrogen bond interactions were considered particularly important for the following reason. Interhelical hydrogen bonds have been shown to be critical in maintaining inactive conformations of G-protein-coupled receptors.²⁸ For rhodopsin, whose structure-function relationships have been studied widely using biochemical and spectroscopic methods, movement of TM3 and TM6 helices is known to produce changes in loop conformations.²⁹ This interhelix movement takes place due to the loss of hydrogen bond interactions between TM3 and TM6 residues. The loss of hydrogen bond network between transmembrane helices, mediated through water molecules, has also been thought to be responsible for carrying out changes in the loop conformations with functional implications.³⁰ When AK530 and AK317 were bound to CCR5, Y108 rotated away from Y251, and the hydrogen bonds between Y108 and E283 and between E283 and S180 were lost (see below). The change in this polar interaction might be responsible for changes in CCR5 loop conformation inhibiting gp120 interaction.

Activity against R5-HIV-1 and the CCR5-binding affinity of CCR5 inhibitors

We determined the activity of two novel SDP-based CCR5 inhibitors, AK530 and AK317 (Fig. 1), against R5-HIV-1 on a cell-based acute R5-HIV-1 exposure assay using the HeLa-CD4-LTR- β -gal indicator cell line expressing human CCR5 [CD4⁺CCR5⁺ MAGI cells] and phytohemagglutinin (PHA) peripheral blood mononuclear (PBM) cells as target cells with two different R5-HIV-1 species, HIV-1_{REF} and HIV-1_{Ba-L}. We also conducted a saturation binding assay using ³H-labeled AK530 and AK317 and CCR5_{WT}-expressing Chinese hamster ovary (CHO) cells, and determined their binding affinity for CCR5_{WT} (K_d ; dissociation constant values), as previously described.¹⁴ As shown in Table 1, AK530 exerted potent antiviral activity against both HIV-1_{REF} and HIV-1_{Ba-L} in two different target cells, with IC_{50} values ranging from 2.1 nM to 32 nM, and proved to have a high binding affinity for CCR5, with a K_d value of 1.4 ± 0.9 nM. AK317 was comparably potent against the virus (IC_{50} = 1.5–25 nM), but had a lower CCR5-binding affinity than AK530 by about a factor of 10 (K_d = 16.7 ± 7.5 nM). Neither of these CCR5 inhibitors had activity against X4-HIV-1 (data not shown). For comparison, the antiviral potency and binding affinity of APL¹⁴ are illustrated in Table 1. APL had greater anti-HIV-1 activity (IC_{50} = 0.2–0.7 nM) than AK530 and AK317, but its binding affinity (K_d = 3.6 ± 1.3 nM) was slightly less than that of AK530.

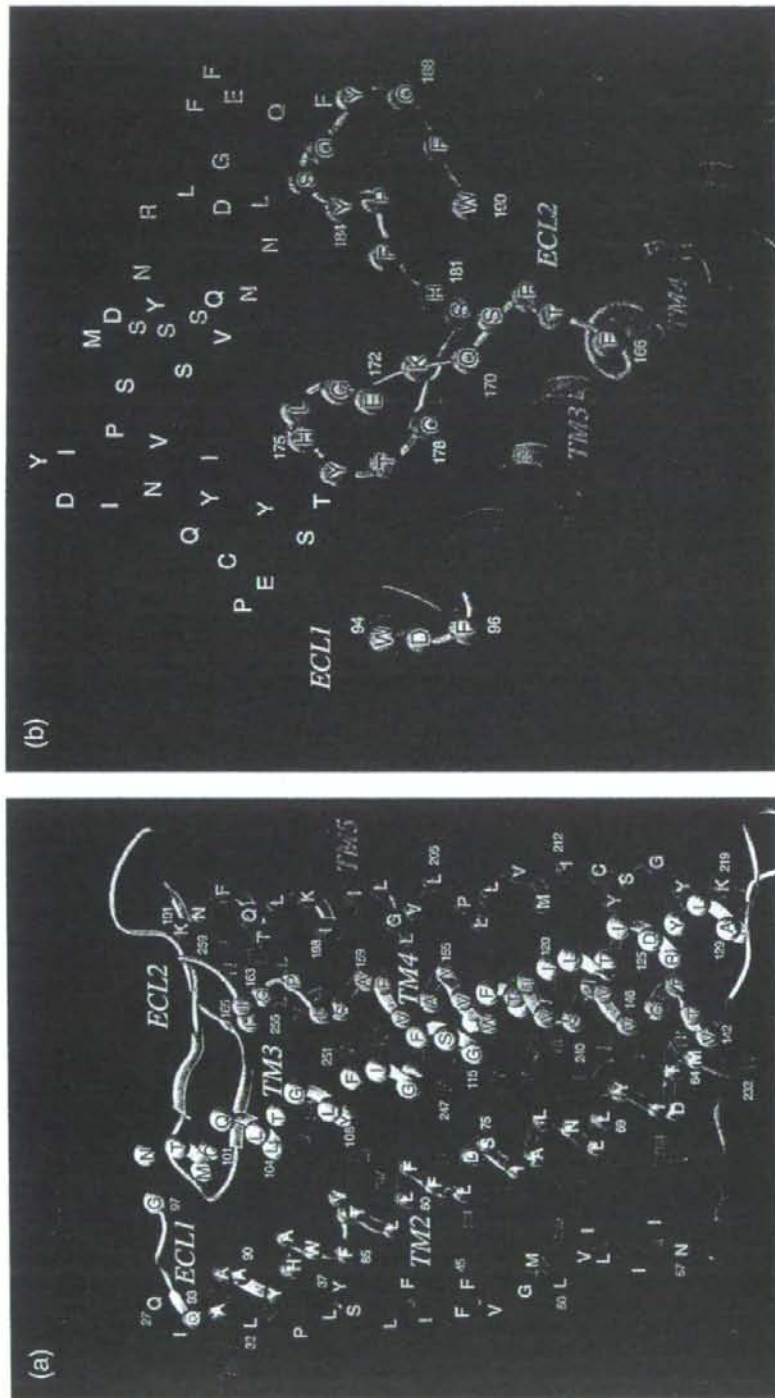


Fig. 2. The transmembrane helices and extracellular loop regions of CCR5. (a) A side view of the transmembrane domains. TM2, TM3, and TM4 are above the plane of the paper, and TM6 and TM7 are below the plane. The following assignments have been made for transmembrane helices: TM1, residues 27–57; TM2, residues 64–93; TM3, residues 97–130; TM4, residues 142–165; TM5, residues 191–219; TM6, residues 232–259; TM7, residues 279–300. (b) A top view of the extracellular loop regions. The following assignments have been made for loops: N-terminus, residues 1–26; first extracellular loop, residues 94–96; ECL2, residues 166–190; third extracellular loop, residues 260–278.

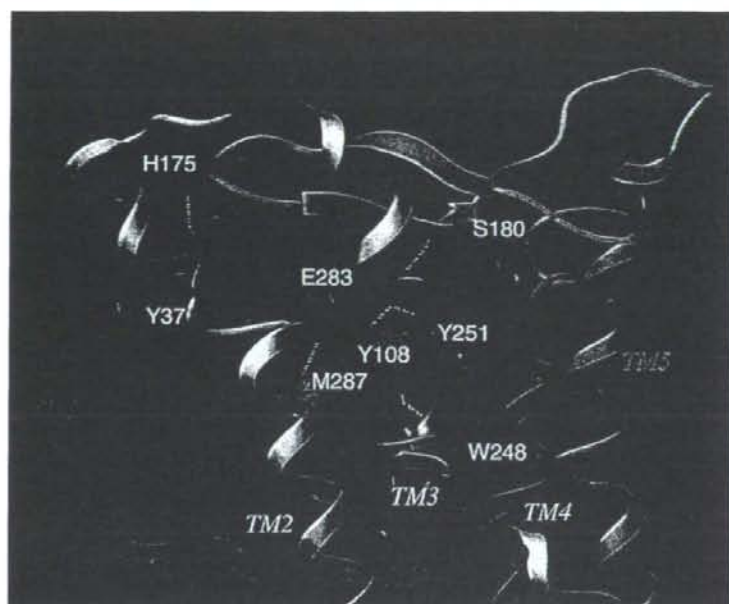


Fig. 3. Transmembrane residues Y108(TM3)/E283(TM7)/Y251(TM6)/M287(TM7)/S180(ECL2) of unliganded CCR5, forming a hydrogen bond network. Y37 has a hydrogen bond interaction with H175. This shows that transmembrane residues, which have been implicated in CCR5 inhibitor binding, have direct interactions with ECL2 residues in the unliganded receptor. It is assumed that these intramolecular interactions are responsible for maintaining a conformation of ECL2 that is favorable for binding with the HIV-1-gp120/CD4 complex. AK530 interacts with Y37, Y108, E283, and Y251 in the binding cavity and disrupts the intramolecular interactions of Y108 and Y251 with E283, and those of E283 with the ECL2 (Fig. 5). It is assumed that these structural changes, after inhibitor binding, alter the conformation of the ECL2, resulting in loss of association with gp120. The analysis strongly suggests that the loss of hydrogen bonds between helices may cause allosteric conformational changes in ECL2, leading to the inhibition of HIV-1 gp120 binding to CCR5.

Profiles of the binding affinity of [³H]AK530 and [³H]AK317 for a panel of mutant CCR5-expressing cells

In order to explain the difference in the anti-HIV-1 activity and CCR5-binding profiles described above, we determined the binding affinity of [³H]AK530 and [³H]AK317 by employing a panel of mutant CCR5-overexpressing CHO cells. As shown in Table 2, we found that the K_d values of AK530 drastically increased, as examined in CHO cells expressing such CCR5 mutations as Y37A, C101A, F109A,

G163R, C178A, T195P, T195S, and Y251A, with all K_d values being >100 nM (>71-fold greater than that with CCR5_{WT}). AK317, whose affinity for wild-type CCR5 was nearly 10-fold lower than AK530, also had a significant decrease in its binding affinity with these mutations, with all K_d values being >100 nM (>5.9-fold greater than that with CCR5_{WT}). As for G163, a Gly-to-Arg substitution was examined in this study because the G163R substitution has been reported to reduce susceptibility to HIV.³¹ In addition, AK317 had a significantly decreased binding affinity for CCR5 when it contained P84H, Y108A, K191A/N, I198A,

Table 1. Anti-HIV activity against WT-R5-HIV-1 and binding affinity for WT-CCR5 of CCR5 inhibitors

Compound		Antiviral assay (virus) [nM]			Binding assay (K_d) [nM]
		MAGI with HIV-1 _{RF1}	MAGI with HIV-1 _{Ba-L}	PHA-PBM with HIV-1 _{Ba-L}	
AK530	IC ₅₀ ^a	2.8±1.5 ^b	2.1±1.1	32±27	1.4±0.9
	IC ₉₀	51±2.5	79±34	430±113	
AK317	IC ₅₀	2.0±0.2	1.5±1.9	25±8	16.7±7.5
	IC ₉₀	19±14	25±3	171±45	
APL	IC ₅₀	0.2±0.1	0.2±0.1	0.7±0.4	3.6±1.4
	IC ₉₀	1.8±0.7	2.9±1.6	12±10	

^a IC₅₀ values were determined with the MAGI assay and the PHA-PBM (p24) assay (see Materials and Methods).

^b The numbers denote the IC₅₀, IC₉₀, or K_d values (mean±SD).

Table 2. Binding affinity of CCR5 inhibitors for mutant CCR5

Mutant CCR5 in CHO cells		K_d value [nM]		
		AK530	AK317	APL
Wild type				
D11A	<i>NH₂ terminus</i>	1.4±0.9	16.7±7.5	3.6±1.4
Y37A		1.1±0.5	14.6±1.9	3.0±0.6 ^a
P84H	TM1	>100	>100 ^b	12.8±0.9
C101A	TM2	37.3±6.3	>100	>100
L104D	TM3	>100	>100	>100
Y108A	TM3	6.8±0.7	93.3±26.4	18.3±3.6
F109A	TM3	60.7±26.2	>100	19.8±4.4^a
F112L	TM3	>100	>100	>100
F112Y	TM3	5.4±2.1	14.7±2.5	4.0±2.6 ^b
F113A	TM3	5.2±3.4	21.1±8.9	6.8±1.1 ^a
F113Y	TM3	2.4±0.3	43.3±7.4	13.3±2.3 ^a
G163A	TM3	2.8±0.5	48.2±10.2	12.9±3.1
G163R	TM4	5.9±2.6	14.7±0.1	8.0±4.2 ^a
R168A	TM4	>100	>100	>200 ^a
K171A/E172A	ECL2	2.2±0.7	24.6±4.1	14.1±9.4
C178A	ECL2	3.5±1.2	14.7±0.1	2.8±0.1 ^a
S180A	ECL2	>100	>100	>200 ^a
S180T	ECL2	7.4±1.4	34.5±7.9	5.7±1.2 ^a
S180E	ECL2	1.4±0.6	14.9±1.7	1.5±0.6 ^a
Y184A/S185A	ECL2	5.7±2.3	61.8±22.9	13.9±1.7 ^a
Y184A/S185A/Q186A/Y187A	ECL2	2.2±2.3	14.8±0.2	2.0±0.8 ^a
Q186A/Y187A	ECL2	2.2±0.4	22.0±4.2	2.0±0.6 ^a
Q188A	ECL2	2.3±0.1	14.4±2.2	2.8±0.5 ^a
K191A	ECL2-TM5	1.9±1.3	14.6±3.6	6.6±1.4 ^a
K191R	ECL2-TM5	6.0±3.8	>100	>200 ^a
K191N	ECL2-TM5	5.2±2.8	22.2±7.7	9.0±5.6 ^a
T195A	ECL2-TM5	12.5±3.3	>100	14.2±1.1 ^a
T195P	TM5	5.6±3.9	14.7±0.1	48.1±4.3
T195S	TM5	>100	>100	>100
K197A	TM5	>100	>100	>100
I198A	TM5	7.6±3.7	58.3±18.7	10.7±3.5
W248A	TM5	9.8±2.2	>100	24.6±4.8^a
Y251A	TM6	43.4±4.5	>100	29.8±4.6
E283A	TM6	>100	>100	36.5±9.5^a
M287A	TM7	19.1±2.5	>100	>200 ^a
M287E	TM7	2.4±1.4	16.1±2.1	6.8±2.3 ^a
		62.7±17.8	87.1±0.6	14.8±1.7^a

^a Data from Maeda *et al.*²²^b K_d values more than fivefold that of CCR5_{WT} are shown in boldface.

W248A, or E283A (all K_d values >100 nM). It was seen that APL significantly decreased its binding affinity (K_d values of >100 nM, >27-fold lower than that with CCR5_{WT}) for CCR5 when it contained a P84H, C101A, F109A, G163R, C178A, K191A, T195P/S, or E283A substitution. Thus, AK317, whose CCR5-binding affinity for CCR5_{WT} was >4-fold lower than that of APL, had virtually the same binding profile as that of APL, while two additional mutations (Y108A, and Y251A), which decreased the CCR5-binding affinity of APL (K_d values <100 nM), also nullified the CCR5 binding of AK317, consistent with the notion that the affinity of AK317 for CCR5_{WT} is lower than that of APL. It was noted that as the K191A substitution significantly reduced the CCR5-binding affinity of both AK317 and APL, it had moderately (4.2-fold) reduced the binding affinity of AK530. Moreover, the Y37A substitution, which caused only a <4-fold reduction in the CCR5 binding of APL (Table 2), produced a significant reduction in the CCR5 binding of AK530 and AK317. Other dissociations in the K_d profiles between APL and AK530 were seen when CCR5 had an amino acid substitution at Y108A (5.5-

fold for APL versus 43.3-fold for AK530), Y251A (10.1-fold for APL versus >71-fold for AK530), or E283A (>55-fold for APL versus 13.6-fold for AK530). Taken together, the results obtained with the saturation binding assay using the ³H-labeled CCR5 inhibitors employed here suggest that the binding profile of AK317 is similar to that of APL; the binding profiles of AK530 and APL share some common features and possibly have some important differences, while both AK530 and AK317 are comparably potent against R5-HIV-1.

Amino acid residues of CCR5 crucial for the interactions with CCR5 inhibitors

We subsequently defined a three-dimensional model of human CCR5-CCR5 inhibitor complex by combining the results of the site-directed-mutagenesis-based analyses described above (Table 2) and molecular modeling that involved structural refinement and docking of inhibitors to an initial structure of CCR5 based on the crystal structure of bovine rhodopsin.^{30,32}

Of note, both amino acid substitutions C101A (TM3) and C178A (ECL2) virtually nullified the binding of all three CCR5 inhibitors examined: AK530, AK317, and APL (Table 2). These findings confirmed the assumption that C101 and C178 form a disulfide bond that is crucial in maintaining the conformation of the ECL2. These data also strongly suggest that either of the two amino acid substitutions disrupted the disulfide link, altered the conformation of the loop, and nullified the binding of the three CCR5 inhibitors to CCR5. This binding profile common to AK530, AK317, and APL indicates that their binding to CCR5 is sensitive to the ECL2 conformation and significantly differs from the binding profile of other CCR5 inhibitors such as SCH-C and TAK-779, which do not undergo drastic loss in their CCR5 binding with these mutations.^{19,22,23}

The model of CCR5 complexed with a CCR5 inhibitor that we generated in the present study was derived by taking the flexibility of both CCR5 and the inhibitor into account and by computationally designing a model that most suitably provided a rational explanation of the mutagenesis data. In the present study, we chose a few CCR5 residues, which were predicted to have significant interactions with the inhibitor based on our initial model.²² The residues chosen for mutation were P84, L104, F109, T195, and W248. P84 was observed to be in close contact with APL in these models (Fig. 4c), and CCR5 containing a P84H substitution (CCR5_{P84H}) was generated. The binding affinity of APL for CCR5_{P84H} decreased by nearly 30 times compared to wild-type CCR5 (CCR5_{WT}) and confirmed that the binding of APL is indeed dependent on this residue (Table 2). L104 was

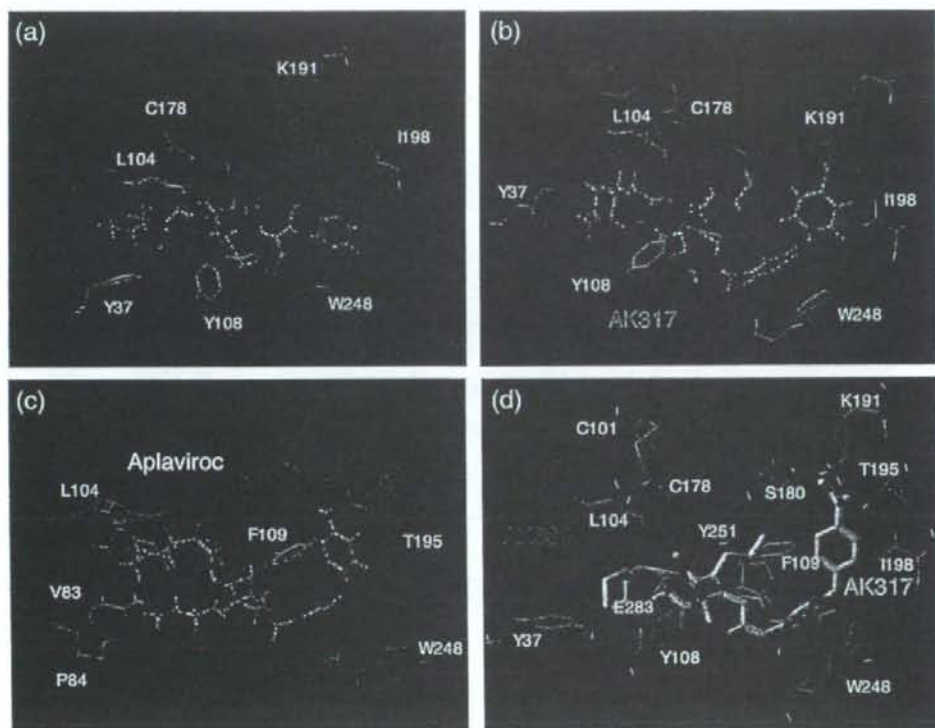


Fig. 4. Lipophilic potential mapped on the binding cavity of CCR5 inhibitors. The lipophilic potential mapped onto the binding cavity when AK530, AK317, and APL bind to CCR5 are shown in (a), (b), and (c), respectively. The predominantly lipophilic region of the cavity is shown in brown (bottom region of the cavity, which is located towards the cytoplasmic region of CCR5). The blue regions are predominantly hydrophilic (present towards the extracellular region), and the green regions are moderately lipophilic. The figure was generated using MOLCAD. The shapes of the binding cavity are slightly different for AK530 and AK317, as receptor conformations are slightly different when these molecules bind to CCR5. The unoccupied volumes of the cavities suggest optimization ideas for improving the potency of these molecules. (d) The binding modes of AK530 and AK317 superimposed. AK530 is shown in red, and AK317 is shown in green. Note that the binding orientations in the vicinity of transmembrane helices 5 and 6 differ. AK317 binds towards and around ECL2 residues, whereas AK530 bends towards the intracellular domain. AK530 has a high binding affinity probably because it binds "deeper" into the cavity. On the other hand, by being able to interact with ECL2 residues, AK317 maintains comparable anti-HIV-1 potency with AK530 even though its binding affinity is about 10-fold lower.

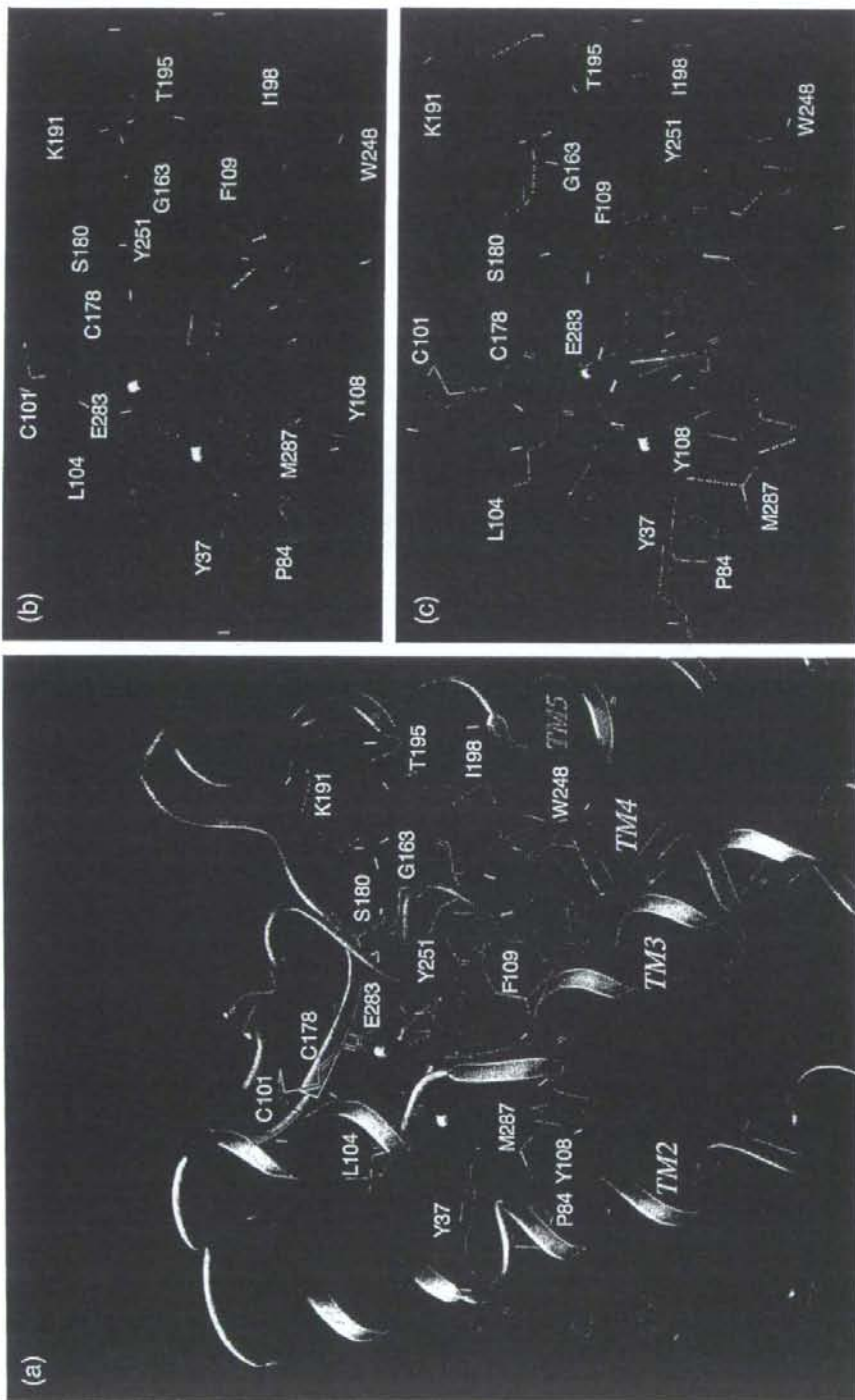


Fig. 5. Amino acid residues forming the binding cavity within CCR5 for AK530. (a) The amino acid residues forming the binding cavity of CCR5 and the binding mode of AK530 are shown. The transmembrane regions and the ECL2 enclose the cavity. Every transmembrane helix has at least one residue that contributes towards forming the binding pocket for AK530. (b) AK530 is predicted to have hydrogen bond interactions with Y37(TM1), Y251(TM6), and E283(TM7), and has favorable hydrophobic interactions with several binding site residues, including P84, L104, F109, and I198. The benzene ring of AK530 forms a π - π interaction with W248. (c) The hydrogen bond networks, involving multiple transmembrane domains, define the shape of the CCR5 cavity for AK530. There is one network of hydrogen bonds involving Y37(TM1), M287(TM7), and Y108(TM3). Another network involves S180(ECL2), G163(TM4), K191(TM4), and T195(TM5). The hydrogen bond networks are different for the unbound and inhibitor-bound CCR5.

also in the proximity of APL-binding cavity (Fig. 4c), and CCR5^{L104D} was generated, proving a decrease in the binding affinity of APL by about fivefold (Table 2). The binding affinities of SCH-C and TAK-779 for CCR5^{P84H} and CCR5^{L104D} were also determined, and there were minimal changes from the wild-type binding affinity (K_d changed by only twofold to threefold). This indicates that P84 and L104 are likely in close contact with APL, and the decrease in the binding affinity of CCR5^{P84H} and CCR5^{L104D} mutants is not predominantly due to any drastic conformational changes that might have accompanied these mutations. The models examined in this study showed that F109 forms a π - π interaction with APL (Fig. 4c). F109 is present in a cluster of aromatic residues involving other nearby phenylalanine and tyrosine residues in the binding pocket. CCR5^{F109A} was generated, proving a drastic loss of APL, AK317, and AK530 binding to CCR5 (Table 2). SCH-C and TAK-779 also had K_d values higher than 100 nM, indicating that F109 is important for the binding of structurally diverse CCR5 inhibitors. T195 was chosen because it was observed that the inhibitors were shown to have different dependences on their binding affinity for this residue. The model for APL (Fig. 4c) showed that an intramolecular hydrogen bond network involving S180/G163/K191/T195 is important for defining the binding cavity for APL, and APL *per se* also has a potential hydrogen bond interaction with T195 (Fig. 4c). The intramolecular hydrogen bond network of CCR5 was not observed in our models of CCR5 complexed with SCH-C or TAK-779. Moreover, SCH-C or TAK-779 does not have any groups or atoms capable of forming hydrogen bond interactions with T195. Indeed, the K_d values for APL for CCR5^{T195P} and CCR5^{T195S} were >100 nM (Table 2), while the binding profile of SCH-C and TAK-779 to CCR5 was not affected by T195P or T195S substitutions [K_d values of SCH-C: 16.0 nM (wild type), 28.9 nM (T195P), and 21.7 nM (T195S); K_d values of TAK-779: 30.2 nM (wild type), 31.1 nM (T195P), and 32.5 nM (T195S)]. Interestingly, in CCR5 complexed with AK530 and AK317, the hydrogen bond network with S180, G163, K191, and T195 was seen, suggesting that the network led to maintain a conformation of CCR5 suitable for the binding of SDP-based inhibitors. Indeed, both AK530 and AK317 failed to bind to CCR5^{T195P} and CCR5^{T195S}, although AK530 did not have a direct interaction with the network (Fig. 5). Taken together, these results sustained our notion that the CCR5 inhibitor-CCR5 interactions generated based on the rhodopsin crystallographic data are reasonably reliable.

Structural analysis of AK530 and AK317 interactions with CCR5

The structural interactions of AK530 with CCR5 are shown in Fig. 5a-c. The binding cavity of AK530 involves residues from each of the transmembrane domains and the ECL2. The binding cavity is stabilized by several intramolecular hydrogen bonds involving residues in different transmembrane regions. Y37, M287, and Y108, which are in transmembrane

helices 1, 7, and 3, respectively, form a hydrogen bond network that defines one end of the cavity. Another network involves S180(ECL2), G163(TM4), K191(TM5), and T195(TM5). AK530 binds in a somewhat diagonal fashion, reaching deeper into the cavity of CCR5, and has several polar and nonpolar interactions that give rise to its very high affinity ($K_d = 1.4$ nM). The hydroxymethylene of AK530 is predicted to have a hydrogen bond interaction with the side chain of Y37, and the diketopiperazine ring of AK530 is predicted to have a hydrogen bond interaction with the side chains of Y251 and E283. The hydrophobic interactions that stabilize binding involve P84, L104, and I198. There are π - π interactions involving F109 and W248. Indeed, the binding affinity of CCR5 species containing Y37A, Y108A, or W248A was drastically reduced in our saturation binding assays, and the residues implicated in the binding of AK530 as described above appear to have an important structural significance. F109 is present in a cluster of aromatic residues in TM3. W248 is part of a highly conserved set of residues present in the TM6 of class A GPCRs. E283 is the fifth residue in TM7. This position has been shown to be involved in the binding of small-molecule ligands to several chemokine receptors.³³ It is noteworthy that we have demonstrated that the E283 residue is important not only in the binding of other CCR5 ligands such as SCH-C and TAK-779 but also in preserving the C-C chemokine/CCR5 interactions and HIV-1-gp120/CD4 complex binding to CCR5.²²

The binding site residues and the binding mode of AK317 are shown in Fig. 6a and b. AK530 and AK317 are analogues and are expected to share certain common features of CCR5 binding. However, important structural differences were identified between the two analogues. AK530 has a cyclohexyl-hydroxymethyl group, whereas AK317 only has a cyclohexyl-methyl group. AK530 has a phenyl-pyrazol moiety, while AK317 has a phenoxy-benzoic acid group as substituent. The carboxylate group of the benzoic acid in AK317 forms hydrogen bond interactions with S180, K191, and T195. These three residues, along with G163, are involved in an intra-CCR5 hydrogen bond network. Thus, it appears that K191 and T195 are not only important in defining the shape of the cavity but are also involved in directly binding with AK317. AK317 has van der Waals interactions with P84, Y108, I198, and Y251, and π - π interactions with F109 and W248. Another intra-CCR5 hydrogen bond network involving Y37(TM1), E283(TM7), M287(TM7), and Y108(TM3) is responsible for defining the binding cavity. As shown in Fig. 4a and b, the size and shape of the binding cavity of AK530 appear to differ from those of AK317, and the superimposition of the binding modes of AK317 and AK530 clearly shows that although these two inhibitors share certain common binding features, the orientations and topography of these two inhibitors are substantially different (Fig. 4d).

As described above, in spite of sharing a common core, the different substituents make the conformation of these two molecules different, giving rise to differences in structural interactions with CCR5. The binding orientations differ the most around TM5 and

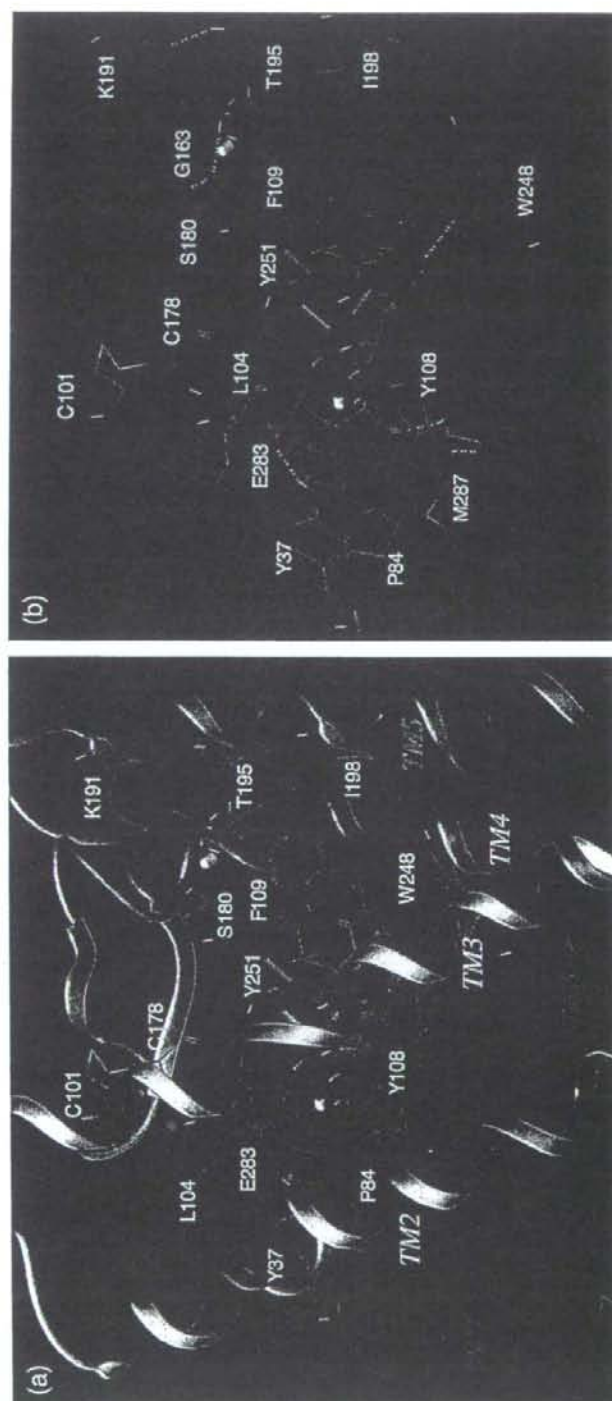


Fig. 6. Amino acid residues forming the binding cavity within CCR5 for AK317. (a) The binding mode of AK317 within CCR5 is shown. (b) The intramolecular hydrogen bond interactions of CCR5 defining the binding cavity and the binding interactions of AK317 with CCR5 are shown. AK317 has hydrogen bond interactions with S180, K191, and T195 (pink dotted line). Other residues in the binding cavity are predicted to have hydrophobic interactions with AK317. As in the case of AK530, there are several intramolecular hydrogen bond networks (yellow dotted line) that define the shape of the CCR5 binding cavity for AK317. There is a network involving S180(ECL2), G163(TM4), K191(TM5), and T195(TM5), and another network involving Y37(TM1), E283(TM7), M287(TM7), and Y108(TM3). The conformation involving amino acid residues in the latter network differs from that of the case of AK530 binding. It appears that CCR5 undergoes different conformational changes to accommodate different inhibitors.

TM6. The phenoxy-benzoic acid group of AK317 interacts with S180 and K191. S180 is a part of ECL2, whereas K191 in TM5 is likely located above the plane of the extracellular region. The pyrazol group of AK530, on the other hand, bends towards the cytoplasmic region and makes the inhibitor bind deeper into the cavity. There are no direct interactions of AK530 with K191, but it seems to be forming a favorable conformation of the binding pocket by an intramolecular hydrogen bond network with G163 and T195 (Fig. 5c). K191, located in the upper domain of TM5, can be considered to be an extracellular residue as well, since a part of K191 is located above the cellular plane (Fig. 2). We speculate that the direct interactions of AK317 with the ECL2 residues such as S180 and with the residues in the extracellular region (such as K191) are responsible for its high antiviral IC_{50} of 2 nM (Table 1). In spite of being a weaker binder compared to AK530, the interactions of the phenoxy-benzoic acid group of AK317 seem to be responsible for its comparable antiviral potency with AK530, which has no direct interaction with ECL2 residues in the vicinity of TM4 and TM5.

The binding cavities of both AK530 and AK317 are mostly lipophilic (Fig. 4a and b). The only strongly hydrophilic regions are towards the extracellular loop region. The shape and volume of the cavities are slightly different for these two inhibitors, as CCR5 is likely to undergo conformational changes to different extents to accommodate these two inhibitors. The unoccupied regions of the cavity suggest new optimization ideas for these inhibitors. For example, substituents of AK530 that can potentially interact with K191 may increase its antiviral potency even further.

Determination of interatomic distances between key amino acids when AK317 and AK530 bind to CCR5

In an attempt to examine whether the binding of AK317 or AK530 to CCR5 causes significant changes in interatomic distances between key amino acids that form the hydrogen bond network seen in the unbound CCR5 as described above (Fig. 3), we carried out molecular dynamics simulation for 4800 ps for AK317- and AK530-bound CCR5, and analyzed critical interatomic distances with the unbound conformation (Fig. 7a-c). In the unbound conformation, Y108 in TM3 was in close proximity to Y251 located in TM6 and had a hydrogen bond interaction with E283 in TM7 (Figs. 3 and 7a and b). In the AK317-bound CCR5, Y108 had rotated away from Y251, and the hydrogen bond interaction between Y108 and E283 was lost. Rotation of Y108 away from Y251 and disruption of hydrogen bond interaction between Y108 and E283 were also observed when AK530 bound to CCR5. TM2 and TM3 can be thought to be in a single plane (above the plane of the paper), and TM6 and TM7 can be thought to be in a different plane (behind the plane of the paper). The rearrangement of Y108 was necessary for the formation of the binding cavity between the transmembrane helices for inhibitor

binding. Furthermore, in the unbound CCR5 structure, E283 is hydrogen-bonded to S180, which is part of the ECL2 (Fig. 3). In fact, E283 moved considerably away from S180 in the inhibitor-bound models of CCR5 (Figs. 5c, 6b, and 7c). Disruption of hydrogen bonds between transmembrane residues and a network of hydrogen bonds mediated through water molecules are known to give rise to the change in the intracellular loop conformation of bovine rhodopsin.^{29,30} Change in ionic interactions between transmembrane residues is also thought to be responsible for the activation of β_2 -adrenergic receptor.³⁴ We speculate that the rotation of Y108 away from the vicinity of Y251, the loss of hydrogen bond interaction between Y108 and E283, and the loss of hydrogen bond interaction between E283 and S180 presumably change the conformation of the ECL2 that is crucial for the binding of the gp120/CD4 complex. These models of unbound and inhibitor-bound CCR5 may give further insights into the mechanism of the inhibition of CCR5 inhibitors involving transmembrane and extracellular residues interacting with each other.

Structural changes in ECL2 caused by CCR5 inhibitors block the binding of CCR5-specific monoclonal antibodies to CCR5

Our structural analyses described above demonstrated that AK530 relatively well maintained its CCR5 binding with the K191A substitution, while AK317 significantly reduced its interactions with CCR5_{K191A}, prompting us to examine whether the different CCR5-binding profiles of these two inhibitors led to different dynamics in their interactions with CCR5-specific monoclonal antibodies (mAbs). To this end, we examined whether AK530 and AK317 blocked the binding to CCR5 expressed on CHO cells of four mAbs: 45531 [specific for the C-terminal half of ECL2 (ECL2B)], 45523 (reactive to CCR5 multidomain), 2D7 [specific for the N-terminus of ECL2 (ECL2A)], and 45549 (reactive to CCR5 multidomain).^{25,35,36} In this mAb-binding blocking assay, the cells were incubated with each inhibitor for 30 min, followed by the addition of a mAb. As shown in Fig. 8, AK317 effectively inhibited the binding of mAb 45531 with an IC_{50} value of 16.3 nM, while the inhibition by AK530 was much less, with an IC_{50} value of 746 nM. AK317 also blocked the binding of mAb 45523 with an IC_{50} value of 282 nM, while AK530 did so with an IC_{50} value of >1 μ M. None of the inhibitors blocked the binding of mAb 2D7 or 45549. When the cells were first exposed to a mAb, followed by the addition of each inhibitor, the resultant inhibition levels were virtually the same (data not shown). Considering that these CCR5 inhibitors are lodged in a hydrophobic pocket at the interface of ECL2 and the upper transmembrane domain (Figs. 4-6), the observed inhibition of mAb binding by CCR5 inhibitors presumably occurred through the allosteric changes secondarily caused by CCR5 binding of the inhibitor, but not through their competition over binding to the antigenic epitope (s) of CCR5.

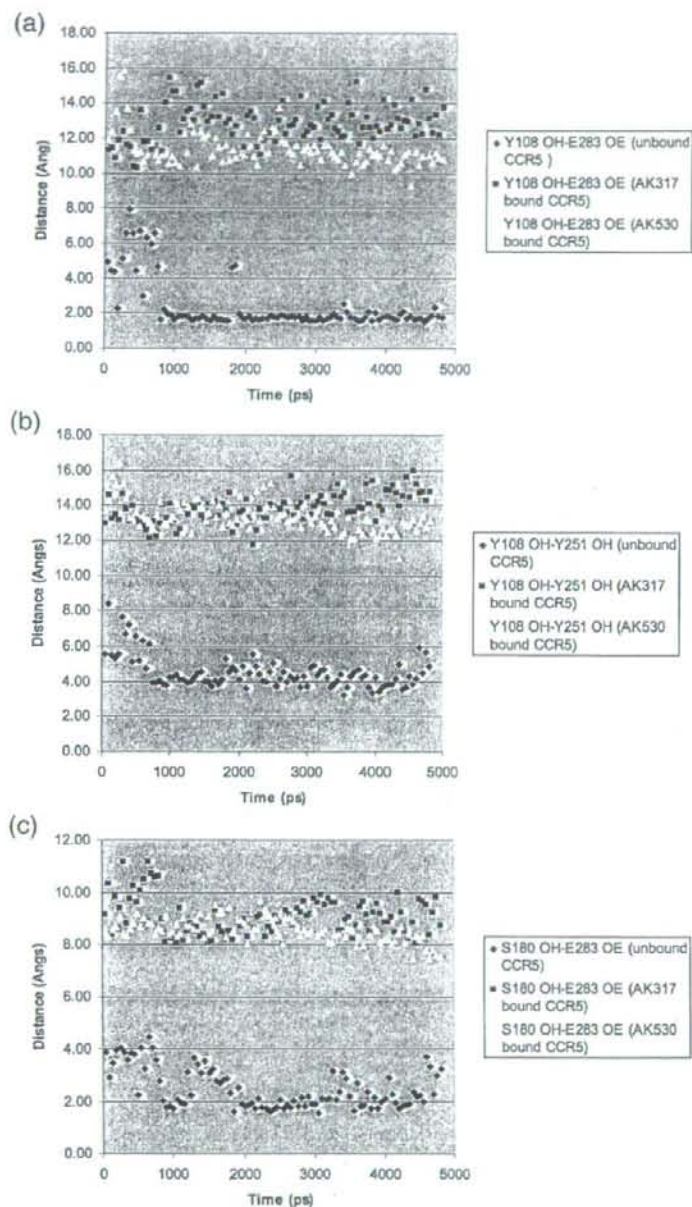


Fig. 7. Key interatomic distances from molecular dynamics simulation of AK317-bound, AK530-bound, and unbound CCR5. Molecular dynamics simulation for AK317- and AK530-bound CCR5 was conducted for 4800 ps, and critical interatomic distances between key amino acids were determined. A hydrogen bond is present if the interatomic distance is <3 Å. (a) Distance between Y108 (hydroxyl hydrogen, PDB atom-type OH) and E283 (carboxylate oxygen, PDB atom-type OE). In the unbound conformation, there is a strong hydrogen bond interaction between Y108 in TM3 and E283 in TM7. Y108 and E283 have to move away from each other to form the binding cavity for the inhibitor to bind, and there is no hydrogen bond between these residues after AK317 and AK530 binding. (b) Distance between Y108 and Y251 hydroxyl oxygen: the tyrosines have moved away from each other after inhibitor binding. (c) Distance between E283 (carboxylate oxygen, PDB atom-type OE) and S180 (hydroxyl hydrogen, PDB atom-type OH). In the unbound conformation, E283 in TM7 has hydrogen bond interactions with S180 in ECL2. This hydrogen bond is disrupted for AK317- and AK530-bound CCR5.

Effects of amino acid substitutions in CCR5 on HIV-1-gp120-elicited cell fusion

In order to better understand conformational changes arising in ECL2 and to determine amino acids that are critical for the cellular entry of HIV-1, we examined the effects of single and multiple amino acid substitutions in ECL2 on HIV-1-gp120-elicited cell fusion. Figure 9 shows the magnitude of cell-cell

fusion between $\text{tat}^+ \text{env}^+ 293\text{T}$ cells and $\text{Luc}^+ \text{CCR5}^+ \text{MAGI}$ cells in the HIV-1-gp120-elicited cell-cell fusion assay. Seven single amino acid substitutions introduced into CCR5 resulted in a substantial reduction ($>70\%$) in the HIV-1-envelope-protein-elicited fusion level (Fig. 9). Three of these single amino acid substitutions (E172A, L174A, and C178A) are located in the ECL2 with an antiparallel β -hairpin structure, while C101A and G163R are in TM3 and TM4, respectively,

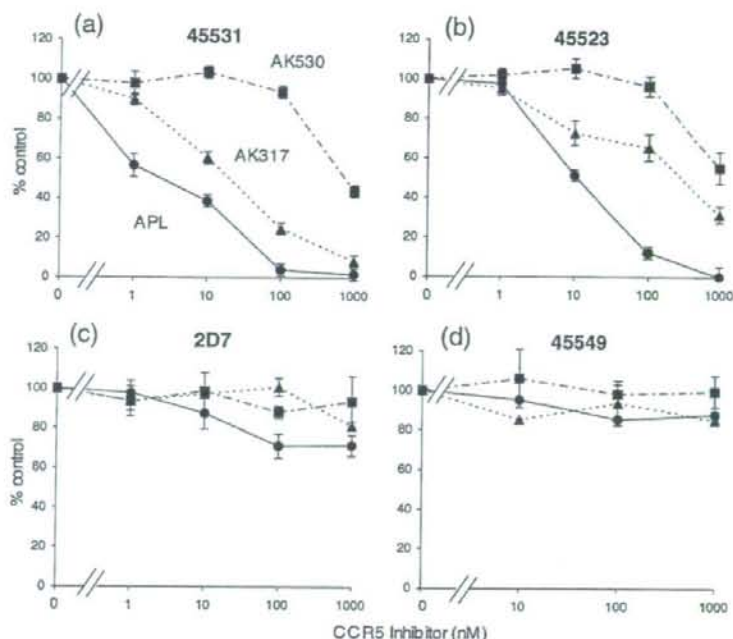


Fig. 8. Inhibition of the binding of anti-CCR5 mAbs by AK530, AK317, and APL. Inhibition by three CCR5 inhibitors of the binding of anti-CCR5 mAbs [45531 (a), 45523 (b), 2D7 (c), and 45549 (d)], which recognize the extracellular domain (s) of CCR5, is illustrated. CCR5-overexpressing CHO cells were incubated with each of the fluorescein-isothiocyanate-conjugated anti-CCR5 mAbs in the presence of various concentrations of a CCR5 inhibitor, and fluorescence intensity on the cells was determined. Each value was compared to that obtained without an inhibitor and is shown as percent control.

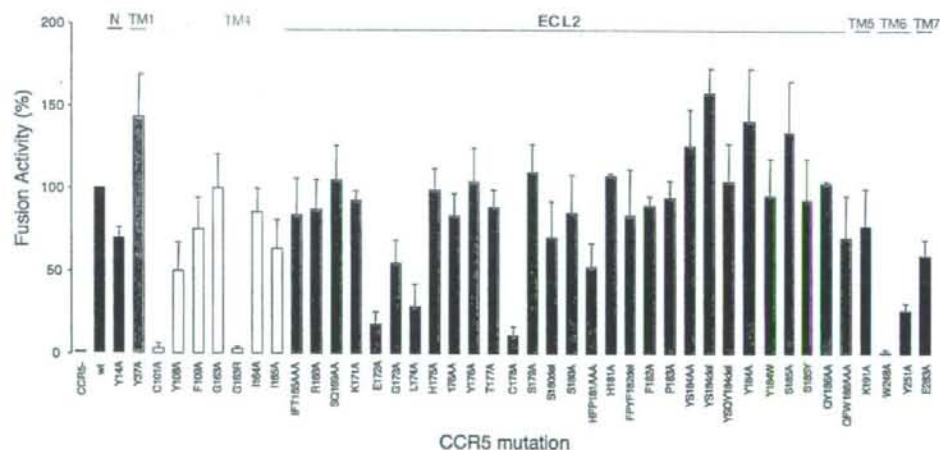


Fig. 9. Effects of amino acid substitution(s) and deletion(s) on HIV-1-gp120-elicited cell-cell fusion. CD4⁺ MAGI cells that expressed sufficient numbers of wild-type or mutated CCR5 were cultured with HIV-1 *env*⁺, *tat*⁺ 293T cells for 6 h, and fusion efficiency was determined with luciferase activity (luminescence levels) using the reporter gene activation assay. The magnitude of luminescence levels with mutant CCR5 is expressed as percent fusion (percent control compared to the luminescence level with wild-type CCR5). Note that three single amino acid substitutions (E172A, L174A, and C178A), which resulted in a substantial reduction in the fusion level (>70%), are located in the ECL2 that has an antiparallel β -hairpin structure (Figs. 2 and 3), while C101A and G163R are in TM3 and TM4, respectively, and W248A and Y251A are in TM6.

and W248A and Y251A are in TM6 (Figs. 2 and 3). Note that E172 is at the NH₂ end of the β -sheet structure of ECL2 and that C178 also belongs to the β -hairpin structural motif (Fig. 2). This finding strongly suggests that these mutations led to the disruption of ECL2's β -sheet structure and resulted in a significant reduction in the cell-cell fusion. Thus, the β -sheet structure of ECL2 seems to be critical for the cellular entry of HIV-1. It is noteworthy that although the two amino acids E172 and L174 do not interact with CCR5 inhibitors (Figs. 4–6), their mutations significantly reduced cell-cell fusion (Fig. 9).

The C101A and C178A substitutions are thought to disrupt the disulfide bond between C101 and C178, which is crucial for the maintenance of the robust ECL2 structure, as demonstrated in this study. Thus, both C101A and C178A substitutions probably led to the aborted HIV-1-envelope-elicited fusion. G163, located in TM4, does not interact directly with AK530, AK317, or APL, but is responsible for maintaining the shape of the binding cavity by its hydrogen bond interactions with S180, K191, and T195 (Figs. 5 and 6). G163R substitution also resulted in virtually a complete loss of fusion (Fig. 9). This is consistent with earlier observations that G163R mutation results in the loss of HIV-1 infectivity.^{22,31}

Amino acids within ECL2 at positions 179 through 190 appeared not to have a crucial role in the HIV-1-envelope-elicited fusion. Indeed, the amino acid substitutions in these positions did not significantly reduce the fusion (Fig. 9). It is noteworthy that these amino acids are located distant from the binding cavity for CCR5 inhibitors (Figs. 2, 5, and 6). It is also of note that W248 has hydrogen bond interactions with Y251 and is thought to play a role in maintaining the conformation of ECL2 (Fig. 3), explaining the reason that W248A substitution results in loss of fusion.

Interestingly, both C178A and C101A substitutions substantially reduced CCR5 binding of the three CCR5 inhibitors (AK530, AK317, and APL), but not that of SCH-C or TAK-779.²² In particular, APL forms hydrogen bonds with C178 and, additionally, has tight interactions with the intramolecular hydrogen bond network (S180/G163/K191/T195).²² AK317 also has interactions with the S180/G163/K191/T195 network (Fig. 6). Thus, SDP-containing CCR5 inhibitors, especially APL and AK317, appear to have greater interactions with ECL2 compared to other non-SDP-containing CCR5 inhibitors such as SCH-C or TAK-779. Our observation that AK530 has the greatest binding affinity for CCR5 (Table 1) but exerts less potent anti-HIV-1 activity (Table 1) may be related to its reduced interactions with ECL2 (Figs. 5 and 7). Such tight interactions with ECL2 may represent a feature conferring potent anti-HIV-1 activity on CCR5 inhibitors, different from allosteric changes caused by CCR5 inhibitors.

Discussion

In the present study, we demonstrated that two novel CCR5 inhibitors, AK530 and AK317, are lodged

in a hydrophobic cavity located between the upper transmembrane domain and ECL2. CCR5 is a member of GPCRs, the largest superfamily of proteins in the body. Understanding the structure of human GPCRs would be invaluable in elucidating their roles in a number of biological processes and should also greatly aid in designing therapeutics. In particular, the elucidation of the detailed structure of human CCR5 and its interactions with HIV-1 envelope glycoprotein should help establish a strategy for HIV-1 intervention. However, no crystal structures of human CCR5 are yet available; bovine rhodopsin and β_2 -adrenergic receptors are the only GPCR species for which crystallographic data have been obtained.^{32,37} Thus, we have previously explored an alternate approach: combination of site-directed-mutagenesis-based saturation binding assay and molecular modeling based on the crystallographic data of bovine rhodopsin.²² The site-directed-mutagenesis-based saturation binding assay alone can give certain insights as to which residues of the receptor are implicated in the binding with the inhibitor. However, it does not indicate which specific atoms of the residue are involved. Homology modeling and docking give insights to interactions between atoms, but these methods produce multiple possible solutions, and it is difficult to differentiate between distinct interactions that are within a small energy range. Combining these complementary methods of site-directed mutagenesis and computational protein structure determination has made it possible to conduct robust structural analyses.²² However, certain validation of the model is crucial. Thus, in the present study, we chose five amino acid residues of CCR5 that were judged to be critical for APL binding based on our previous analysis, and additional mutagenesis studies were carried out. When an amino acid substitution (P84H, C101A, F109A, T195P, or T195S) was introduced into CCR5_{WT} and saturation binding assay was performed using [³H]APL, all K_d values proved to be >100 nM, while the K_d value of [³H]APL with wild-type CCR5 was 3.6 nM. This corroborated the notion that we previously made²²—that the alternate approach using saturation binding assay, combined with our computational protein structure determination, can provide reasonably robust structural insights.

In the present study, we attempted to obtain a refined structural CCR5 model through molecular dynamics computation. In an unbound CCR5, we identified key interactions between residues located in different transmembranes, and between transmembrane and ECL2 amino acid residues. Amino acids involved in such intramolecular interactions included Y37, H175, Y108, Y251, E283, and S180. The intramolecular hydrogen bond interactions observed among different transmembrane regions, and between transmembrane and ECL2 loop presumably stabilize the unbound conformation of CCR5 (Fig. 3). In order to determine the structures of AK317, and AK530 complexed to CCR5, we utilized a novel algorithm to incorporate receptor flexibility and induced-fit effects.³⁸ The optimized AK317-CCR5 and AK530-CCR5 complex structures indica-

ted a rotation of Y108(TM3) away from both Y251 (TM6) and E283(TM7) to make room for the inhibitor within the transmembrane helices. As a result of inhibitor binding, the hydrogen bond between Y108 and E283 and that between E283 and S180 seen in the unliganded CCR5 were disrupted, and these residues formed hydrogen bond or tight van der Waals interactions with the inhibitors instead (Figs. 5–7). The disruption of interhelix residue interactions may cause movement of the transmembrane helices and changes in the conformation of ECL2. A similar mechanism, involving disruption of interhelix hydrogen bond interactions, is thought to be responsible for changes in loop conformation in rhodopsin^{27,29} and in the activation of β_2 -adrenergic receptor.³⁴ Note that Y37(TM1) is involved in a hydrogen bond interaction with ECL2 via H175. We have observed that Y37 interacts with SCH-C and TAK-779.²² These arrangements of hydrogen bond interactions between transmembrane helices and ECL2 should also provide an explanation of the reason that these inhibitors exert potent antiviral activity against HIV-1. Thus, the disruption of hydrogen bond interactions between transmembrane helices, and between transmembrane helices and ECL2, should be a mechanism of allosteric inhibition observed by the binding of CCR5 inhibitors to a binding domain residing mostly within the transmembrane residues.

We also examined the interplays of ECL2 and selected amino acid residues that consist of the largest hydrophobic cavity within CCR5, which accommodate small-molecule CCR5 inhibitors. Our previously published data²² and data by others^{19,23} showed that two CCR5 inhibitors (SCH-C and TAK-779) have no direct interactions with amino acid residues in the extracellular domain, including ECL2. However, all the three SDP-based CCR5 inhibitors that we examined (AK530, AK317, and APL) had substantial interactions with amino acids in ECL2, in particular with C178, which is located in the antiparallel β -hairpin structural motif of ECL2, and with K191, which is located at the interface of ECL2 and TM5 (Figs. 4–6). The C178A substitution virtually abrogated the binding of the three inhibitors to CCR5. C178 is presumed to form a disulfide bond with C101 of TM3 and seems to be critical for the conformation of ECL2. The disruption of the disulfide bond with C178A mutation may result in decreased binding of the three SDP-based inhibitors. Our previous observation²² and the report from others^{19,23} that the same C178A substitution did not affect the CCR5 binding of two other CCR5 inhibitors, SCH-C and TAK-779, suggest that C178 plays a unique but critical role in the binding of AK530, AK317, and APL. In the present study, K191A substitution also virtually nullified the CCR5 binding of AK317 and APL (Table 2), although it did not significantly affect the binding of AK530 probably due to the absence of hydrogen bonding between AK530 and K191 (Fig. 5). Taken together, these data suggest that, unlike the cases of SCH-C and TAK-779, at least a part of the hydrophobic cavity where AK530, AK317, and APL are lodged within CCR5 involves

ECL2. The disruption of ECL2's β -sheet structure by the removal of disulfide bond through C101A and C178A substitutions virtually nullified both the binding of all three CCR5 inhibitors and the HIV-1-gp120-elicited fusion. This strongly suggests that ECL2 plays a crucial role not only in the binding of the three CCR5 inhibitors but also in the interaction of HIV-1 envelope glycoproteins with CCR5. The data also suggest that at least two amino acids in ECL2, C178 and K191, can be potential targets for the design of CCR5 inhibitors.

Several studies have shown that the resistance against a CCR5 inhibitor emerged without the change in coreceptor usage.^{39–44} Resistant R5-HIV-1 variants were reportedly obtained by passage 22 for AD101,⁴⁰ passage 43 for TAK-652,⁴¹ passage 20 for VVC,⁴³ and passages 12–18 for MVC.⁴² However, we have failed in selecting R5-HIV-1 variants resistant to APL even after 60 passages *in vitro* (over ~1.5 years) (Nakata *et al.*, unpublished data), although the possibility of the emergence of HIV-1 variants resistant to APL cannot be ruled out in other settings.⁴⁵ Pugach *et al.* demonstrated that one of the mechanisms by which HIV-1 becomes resistant to CCR5 inhibitors such as VVC is by "noncompetitive resistance"—a process in which a resistant virus continues to enter target cells regardless of the concentration of the inhibitor once HIV-1 has acquired the ability to use the inhibitor-bound CCR5 for entry.⁴⁴ Of note, Westby *et al.* reported that a virus resistant to MVC retained susceptibility to APL, suggesting that the virus can use MVC-bound CCR5 for entry, but cannot use APL-bound CCR5.⁴² Thus, APL is likely to have such a profile that does not allow or delay HIV-1 acquisition of the ability to utilize the "APL-bound" CCR5 for its cellular entry. This potentially favorable property of APL may be related to the direct interactions of APL with amino acids in ECL2, producing "substantially distorted" ECL2 with which HIV-1 gp120 cannot get engaged for its cellular entry, while certain unique allosteric changes in ECL2 conformation following the binding of APL might also explain the substantial delay or lack of the emergence of APL-resistant HIV-1.

The present data, taken together, demonstrate that structural modeling analysis, coupled with CCR5-binding affinity data, should help understand the structural/molecular mechanism of the inhibition of HIV-1 infection by CCR5 inhibitors. The data should not only help delineate the structural dynamics of CCR5 following ligand binding but also aid in the design of therapeutic inhibitors. The data, in particular, demonstrate that by studying the properties of unbound and inhibitor-bound CCR5, transmembrane residues such as Y108, Y251, and E283 are important for gp120 fusion, HIV infectivity,²² and inhibitor binding. The loss of hydrogen bond interactions among these key transmembrane residues and the interactions between E283 and S180, which are essential for the formation and maintenance of the binding pocket for CCR5 inhibitors, might be responsible for changes in ECL2 conformation, providing insights into the mechanism of gp120 inhibition.